ANALYSIS OF ON-AIRCRAFT ANTENNA PATTERNS

W. D. Burnside

Ohio State University

Prepared for:

Naval Air Development Center

May 1973

UNCLASSIFIED

AD777975

DOCUMENT CONTROL DATA - R & D

(Security classification of title, body of abstract and indexing annotation must be entered when the overall report is classified)

1. ORIGINATING ACTIVITY (Corporate author) The Ohio State University ElectroScience Laboratory Department of Electrical Engineering Columbus, Ohio 43212	2a. REPORT SECURITY CLASSIFICATION Unclassified 2b. GROUP

3. REPORT TITLE

ANALYSIS OF ON-AIRCRAFT ANTENNA PATTERNS

4. DESCRIPTIVE NOTES (Type of report and inclusive dates)

Final Report

5. AUTHOR(S) (First name, middle initial, last name)

Burnside, W.D.

6. REPORT DATE May 1973	7a. TOTAL NO. OF PAGES 60	7b. NO. OF REFS 29
8a. CONTRACT OR GRANT NO N62269-72-C-0354 new b. PROJECT NO c d	9a. ORIGINATOR'S REPORT NUMBER(S) ElectroScience Laboratory 3390-2 9b. OTHER REPORT NO(S) (Any other numbers that may be assigned this report)	

10. DISTRIBUTION STATEMENT

Approved for Public Release; Distribution Unlimited

11. SUPPLEMENTARY NOTES	12. SPONSORING MILITARY ACTIVITY Naval Air Development Center Warminster, Pa. 18974

13. ABSTRACT

High frequency radiation patterns of on-aircraft antennas are analyzed using ray optics techniques. This is a basic study of aircraft-antenna pattern performance in which the analytic aircraft is modelled in its most basic form. The fuselage is assumed to be a perfectly conducting convex surface. The wings are simulated by arbitrarily many sided flat plates and the jet engines are treated as finite circular cylinders. The three principal plane patterns are analyzed in great detail with measured results taken to verify each solution. A volumetric pattern study is initiated with the fuselage modelled by an arbitrary convex surface of revolution.

64

DD FORM 1 NOV 65 1473

UNCLASSIFIED
Security Classification

14 KEY WORDS	LINK A		LINK B		LINK C	
	ROLE	WT	ROLE	WT	ROLE	WT
On-Aircraft Antennas						
Radiation Patterns						
Roll Plane						
Elevation Plane						
Azimuth Plane						
Volumetric Patterns						
Geometric Theory of Diffraction						
Modal Solutions						
Experimental Verification						

TABLE OF CONTENTS

I. INTRODUCTION

Radiation pattern analysis of on-aircraft antennas at high frequencies is the object of this research. It is a computer-modelled study of aircraft antenna pattern problems in which the antenna is mounted on the fuselage near the top or bottom. For general applicability, the aircraft is modelled in its most basic form. The fuselage is assumed to be a perfectly conducting convex surface. Thus, the effects of the cockpit and radome are neglected at present.

The need for the type of solution developed in this study is basically two-fold. First, there may be as many as 200 antennas mounted on a single aircraft. If these antennas can be located on the aircraft at the design stage, then one can expect better performance in that optimum locations and structural changes can be found using theoretical solutions of the modelled aircraft under investigation. Secondly, antenna systems are normally added or changed in the course of an aircraft's useful lifetime. Thus, location and relocation of antennas has always required a great deal of time and money. For example, it is not uncommon for one to spend six months building a model and a second six months measuring radiation patterns for antennas mounted at various locations around the structure. On the other hand, it is conceivable that one could accomplish the same result in a fraction of the time (perhaps a day) using computer-simulated models of the aircraft. Once an optimum region is determined the antenna can simply be tested to ascertain its actual performance. Not only can these computer-simulated results be used to determine the location, but they can, also, determine the optimum antenna design for a given application. These analyses employ mutually orthogonal delta function sources to solve for the pattern of an arbitrary fuselage mounted antenna simply through integration over the equivalent aperture currents.

Some of the first solutions used to compute on-aircraft antenna patterns were the modal solutions for infinitely long circular[1,2] and elliptical[3] cylinders. These solutions modelled the fuselage by a cylinder whose elliptical cross-section approximated the fuselage cross-section at the antenna location. Arbitrary antennas were considered in these studies in which the antenna was mounted either on or above the fuselage. These solutions are quite adequate provided the aircraft structure is not illuminated too strongly. However, with the desire to improve system performance, versatility, and coverage the antenna pattern often is shaped for the desired application in such a way that it can actually illuminate the structure quite strongly. In fact, in many cases the system's performance is dependent on the pattern effects of the secondary contributors. For example, too strong a ripple in a pattern may cause a system to function on a secondary lobe rather than the desired main beam. Consequently, the demands of modern sophisticated systems require that the analytic model represent the actual aircraft in more detail than assumed by the modal solutions alone.

With the advent of modern digital computers, one is able to obtain integral equation solutions for antenna patterns and impedance using moment methods. Using this approach the surface currents are assumed to be of a given form and the values of these complex currents are found by forcing the tangential component of the electric field to vanish on the surface. One of the first moment solutions applied to aircraft antenna problems was the wire grid technique using a point matching scheme.[4] This solution requires approximately 100 unknown currents per square wavelength to be found in order that the wire grid adequately model a perfectly conducting surface. A more sophisticated approach has been developed by Richmond[5] which uses a reaction technique to solve for the unknown currents. Yet this solution still requires a wire grid model of the aircraft with approximately 100 unknown currents per square wavelength. An exhaustive study of this aproach has been made by Lin[6] in which he treated the bistatic scattering problem; however, the same conclusions apply for both problems.

A third approach has been developed recently by Richmond in which he divides the surface into patches with each patch having two unknown complex currents. Using this approach only 20 unknown currents per square wavelength need to be found. In other words, one is able to consider a much larger surface using this surface patch solution. However, all of these solutions are restricted to lower frequencies, based on the fundamental limitation on the size of matrices which modern computers can invert without excessive loss of accuracy.

Another approach that has found great success at solving this type of problem is the Geometrical Theory of Diffraction (GTD). GTD is basically a high frequency solution which is divided into two basic problems; these being wedge diffraction and curved surface diffraction. The wedge diffraction solution has been applied to determine the radiation patterns of such basic antennas as parallel plate antennas[7,8,9], parallel plate arrays[10,11], horn antennas[12,13], parabolic reflectors[14,15], and rectangular waveguide antennas[16]. Both of these diffraction solutions have been applied in computing the patterns of antennas mounted on cylinders[17,18,19], rockets[20], and wings[21]. Using this approach one applies a ray optics technique to determine components of the field incident on the various scatterers. Components of the diffracted field are found using the GTD solutions in terms of rays which are summed with the geometrical optics terms in the far field. The rays from a given scatterer tend to interact with the other structures causing various higher-order terms. In this way one can trace out the various possible combinations of rays that interact between scatterers and determine and include only the dominant terms. Thus, one need only be concerned with the important structural scattering components and neglect all other higher-order terms. This makes the GTD approach ideal for a general high frequency study of on-aircraft antennas in that only the most basic structural features of the aircraft need to be modelled.

The basic approach applied here is to decompose the aircraft into its simplest structural forms and analyze these structures using ray optics techniques with numerical values obtained using modal solutions, physical optics, and GTD. Once the scattered fields from these structures are found and verified by measured data, they are adapted to the aircraft model simply by adjusting the incident field. In this way the aircraft begins to grow out of simple forms into a structure that actually resembles a modern aircraft in a general way.

The lower frequency limit of this solution is dictated by the spacings between the various scattering centers in that they should be at least a wavelength apart. In some cases even this requirement can be relaxed. The upper frequency limit is dictated by the analytic model representation as compared with the actual aircraft in that at higher frequencies more of the smaller detail of the aircraft structure should be included in the analytic model.

II. PRINCIPAL PLANE PATTERN ANALYSES

The principal plane pattern analyses were developed primarily under the previous Contract N62269-71-C-0296. However, various improvements have been made that make the previous solutions even more accurate and versatile. A review of these analyses is given here with the improvements considered in more detail. Several results are presented to illustrate the potential of these solutions. The basic aircraft considered in these studies is illustrated in Fig. 1.

Our roll plane pattern solution (x-y plane in Fig. 1) was begun by considering a two-dimensional model composed of circular cylinders simulating the fuselage and engines, with flat plates modelling the wings. From this study[22], it was found that the engines had very little effect with the source mounted near the top or bottom of the fuselage. However, the wing was found to be an important secondary scatterer and must be considered in more detail.

The wing was then modelled by n-sided flat plates. Using the GTD approach, the plate was first isolated, analyzed, and verified by experimental results. Our flat plate solution is compared with the measured pattern from a circular disc in Fig. 2. Note that the agreement between patterns tends to improve as the number of sides is increased. Another example is illustrated in Fig. 3, where the measured and calculated patterns for a dipole above a square plate are compared. Again, good agreement is obtained.

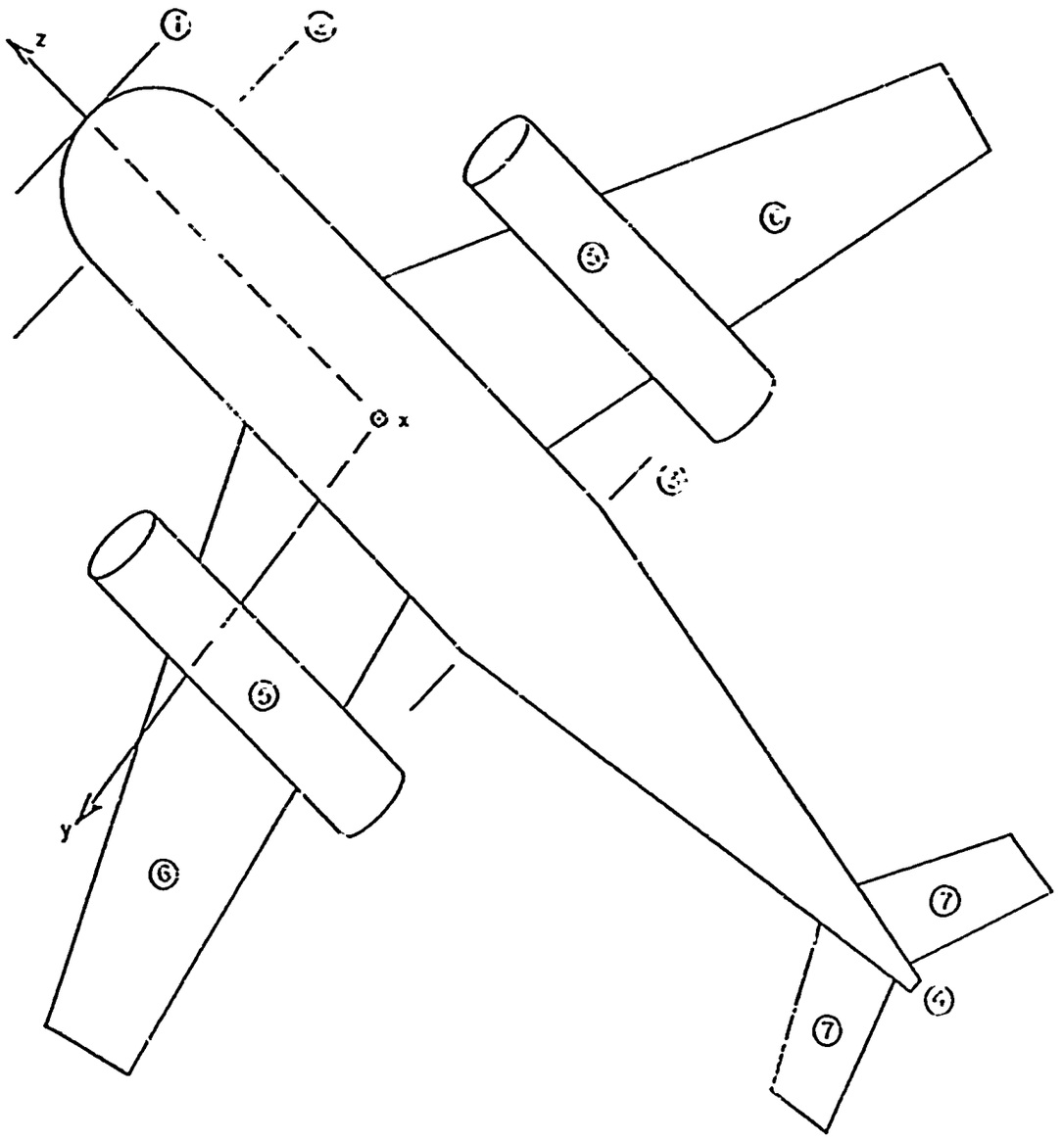

STATION

1-2 SPHERE
2-3 CIRCULAR CYLINDER
3-4 CONE
5 CIRCULAR CYLINDER
6 PLANAR CONDUCTOR
7 PLANAR CONDUCTOR

Fig. 1. Simplified aircraft model.

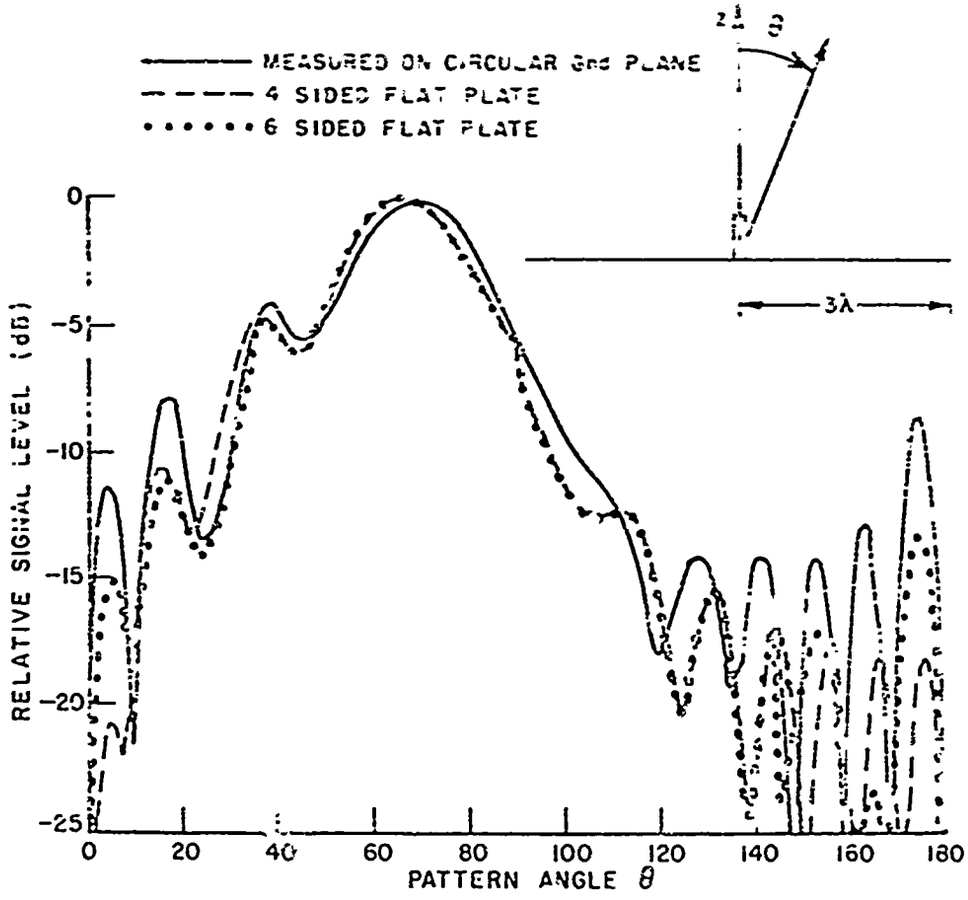

Fig. 2. Radiation pattern of · stub on a ground plane.

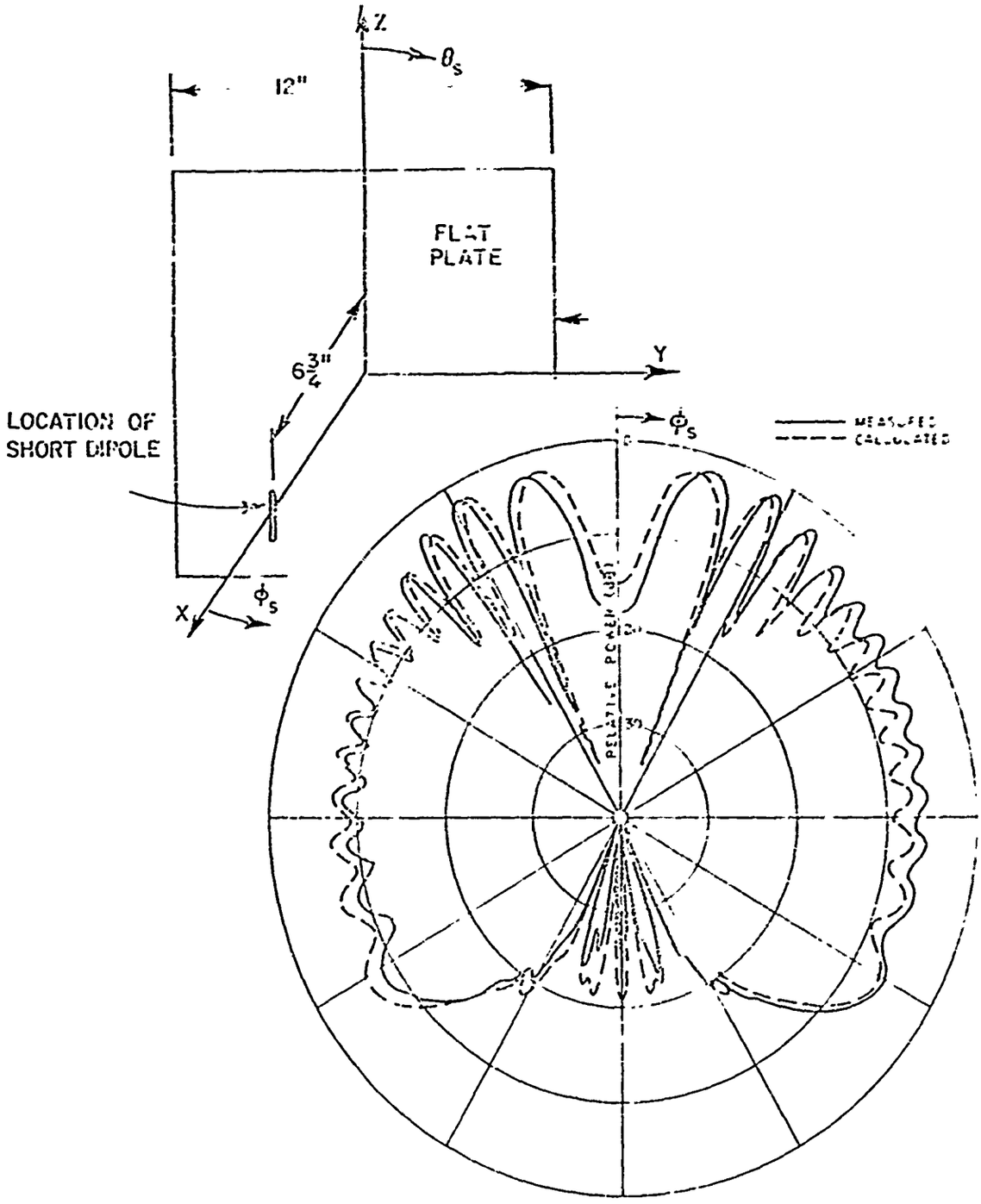

Fig. 3. E_θ radiation pattern for a small dipole mounted above a rectangular plate for $\theta_s = 90°$ and $0° < \phi_s \leq 360°$ at f = 10.43 GHz.

The flat plate model was then applied to an infinitely-long circular cylinder at the central position (Fig. 4a) to form our first three-dimensional roll plane model. The calculated and measured results are presented in Fig. 5 for a short monopole mounted at various locations on this model. In each case the results compare very favorably.

Our first model was a definite improvement over the previously applied infinitely-long cylindrical aircraft model. Under the present contract several modifications were made to improve this model. First, it was found that most aircraft can not, in general, be modelled by a centrally located wing. In order to handle these situations, the model was modified so that the wings could be moved up or down from the central location as illustrated in Fig. 4b and c. The analyses applied for the case with the wings moved upward is presented in Reference [23] with the main consideration being the diffraction from the edge formed by the wing-fuselage junction. This was not a problem for the centrally located wing in that no diffractions occur for the right angle junction. Some examples of this solution are shown in Fig. 6.

Assuming that the diffracted field is negligible from the cylinder-vertical plate junction for the model represented in Fig. 4c with the wings moved down, the solution is essentially identical with that of Fig. 4a. An example of this solution is presented in Fig. 7 for a case with a short monopole mounted directly above the wings which are connected to the fuselage at the bottom of the cylinder. One can, then, compare Figs. 5a, 6a and 7 to observe the effect of the wings placed in a central location, an upward location, and finally, a lower location, respectively.

In each case good agreement has been obtained between our solutions and experimental results taken on models which approximate our aircraft representation. To illustrate the utility of these solutions in solving practical aircraft antenna problems, the analytical results have been compared with experimental results taken on actual scale models. For example, in Fig. 8 the results are compared for a monopole and circumferential slot mounted on an F-4 aircraft. The computed patterns took approximately 30 seconds on the CDC 6600 at Naval Air Development Center. These results indicate that our solutions could have been successfully applied to determine the necessary pattern characteristics for the given cases. Consequently, the solutions appear to be practical as well as efficient.

The second problem that has evolved in our roll plane solution is the effect of having a concave corner in the wing as illustrated in Fig. 9a. This type of wing structure was not considered in our original analysis for the flat plate scattering. The problem arises in determining if the ray from the image source passes through the finite limits of the flat plate (wing).

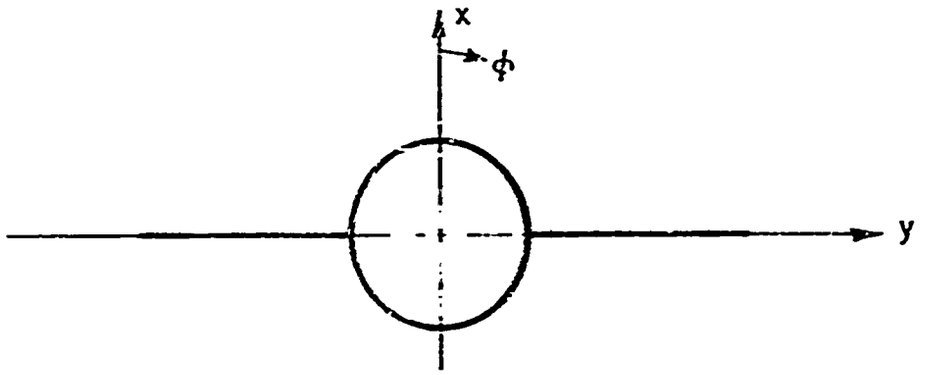

(a) CROSS SECTION OF ROLL PLANE MODEL WITH WINGS IN THE CENTER POSITION

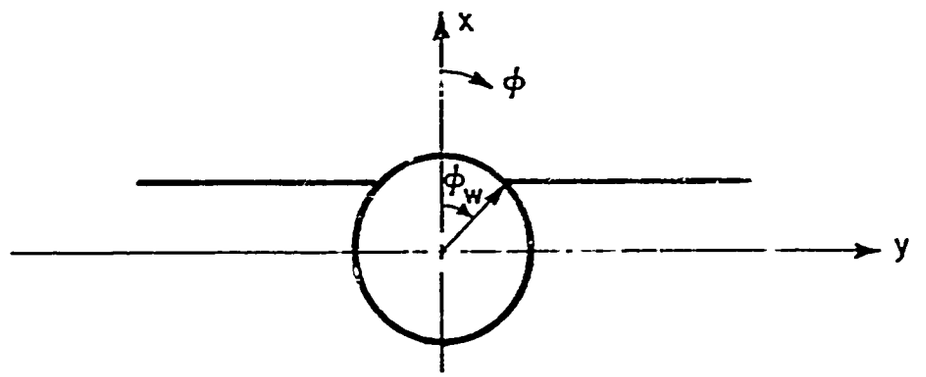

(b) CROSS SECTION OF ROLL PLANE MODEL WITH THE WINGS ABOVE THE CENTER POSITION

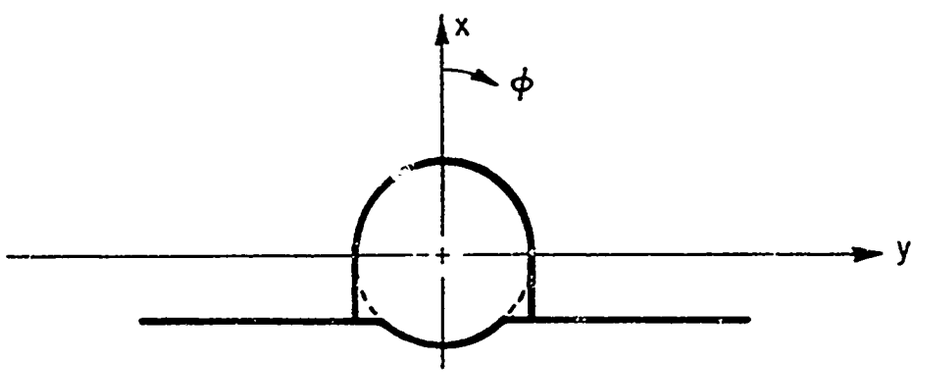

(c) CROSS SECTION OF ROLL PLANE MODEL WITH THE WINGS BELOW THE CENTER POSITION

Fig. 4

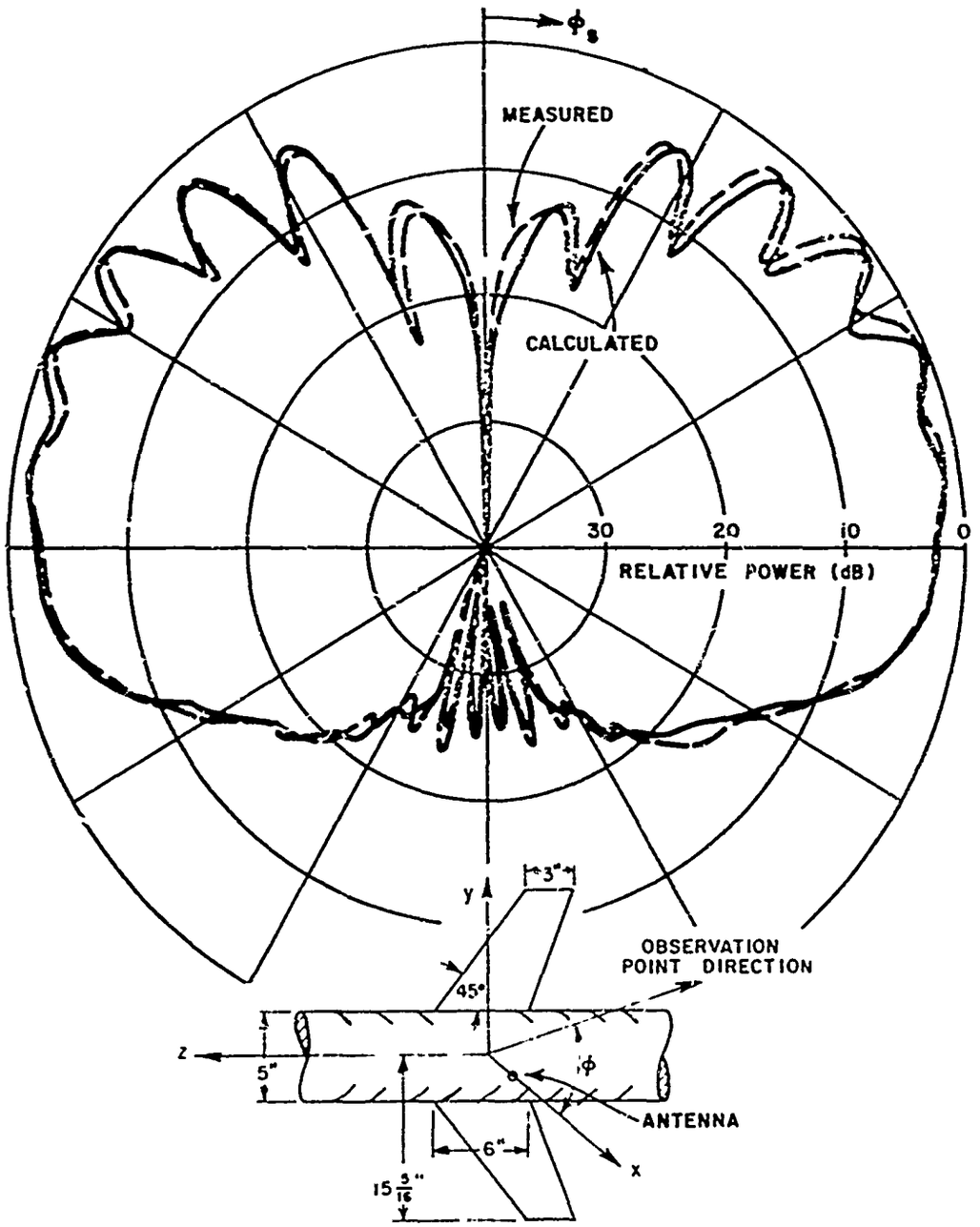

Fig. 5a. Roll plane pattern (E_ϕ) of monopole at point (a_f, $\phi' = 0°$, $z' = 0$) with wings in center position.

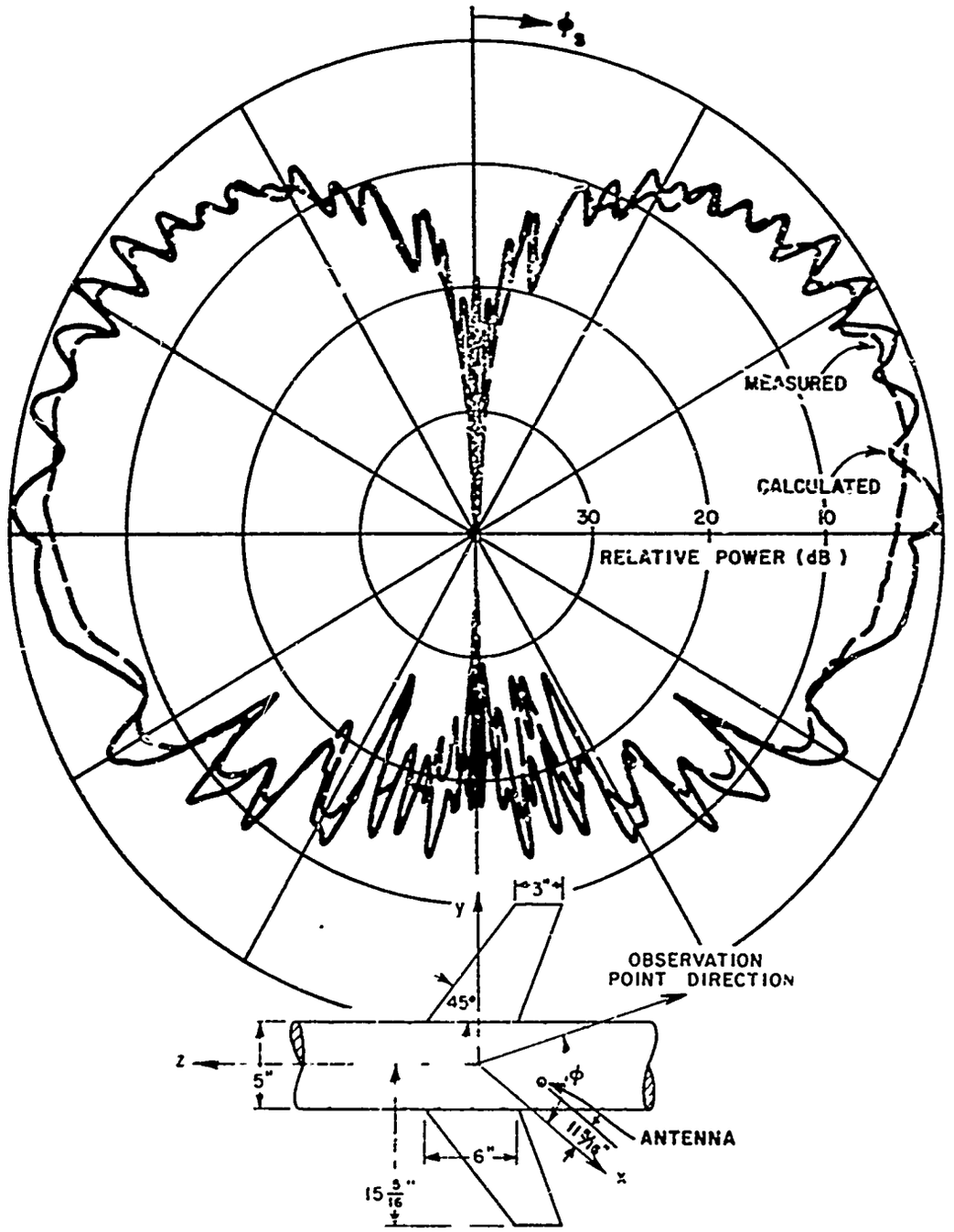

Fig. 5b. Roll plane pattern (E_ϕ) of monopole at point (a_f, $\phi' = 0°$, $z' = 11\,5/16"$) with wings in center position.

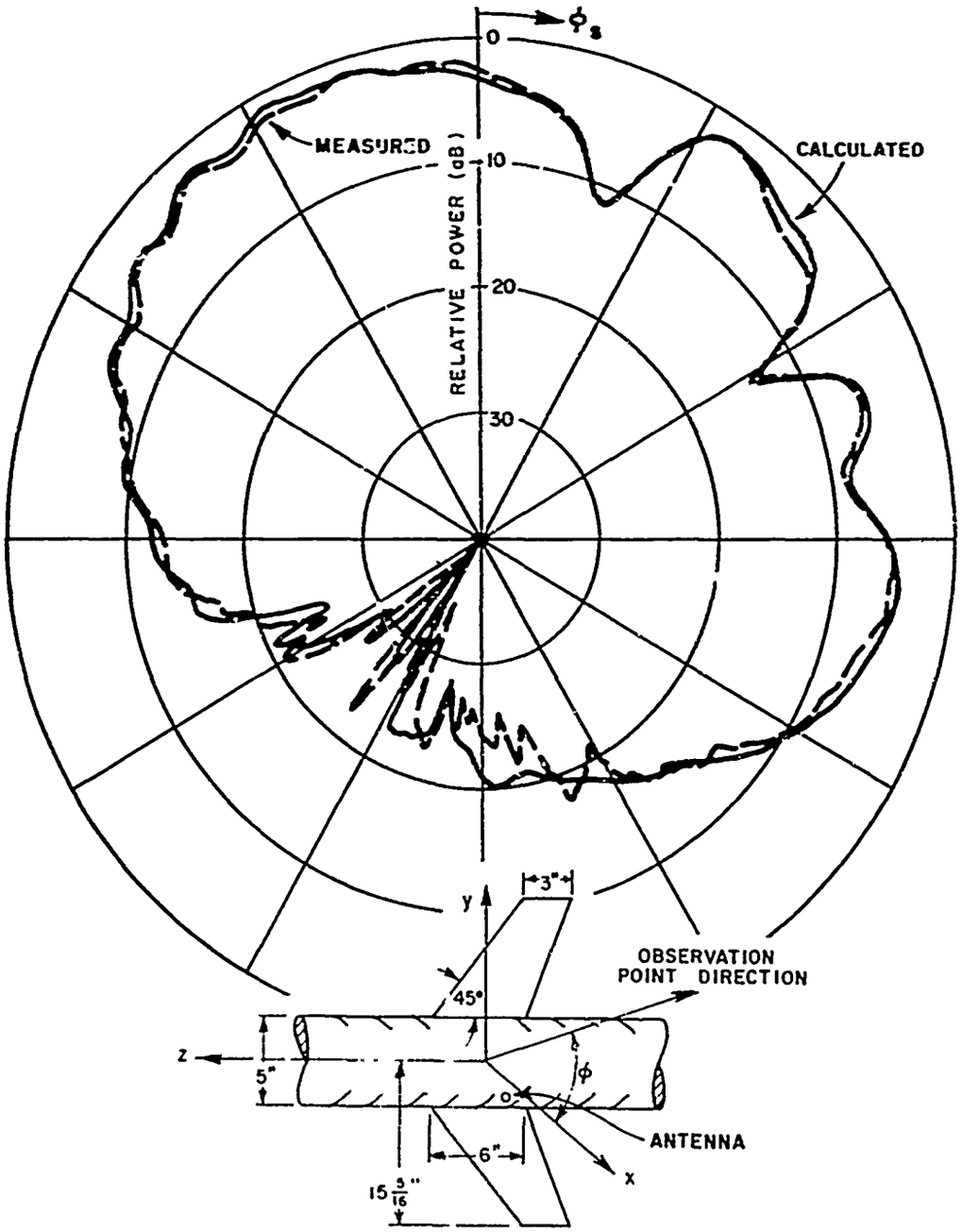

Fig. 5c. Roll plane pattern (E_ϕ) of monopole at point (a_f, ϕ' = 45°, z' = 0) with wings in center position.

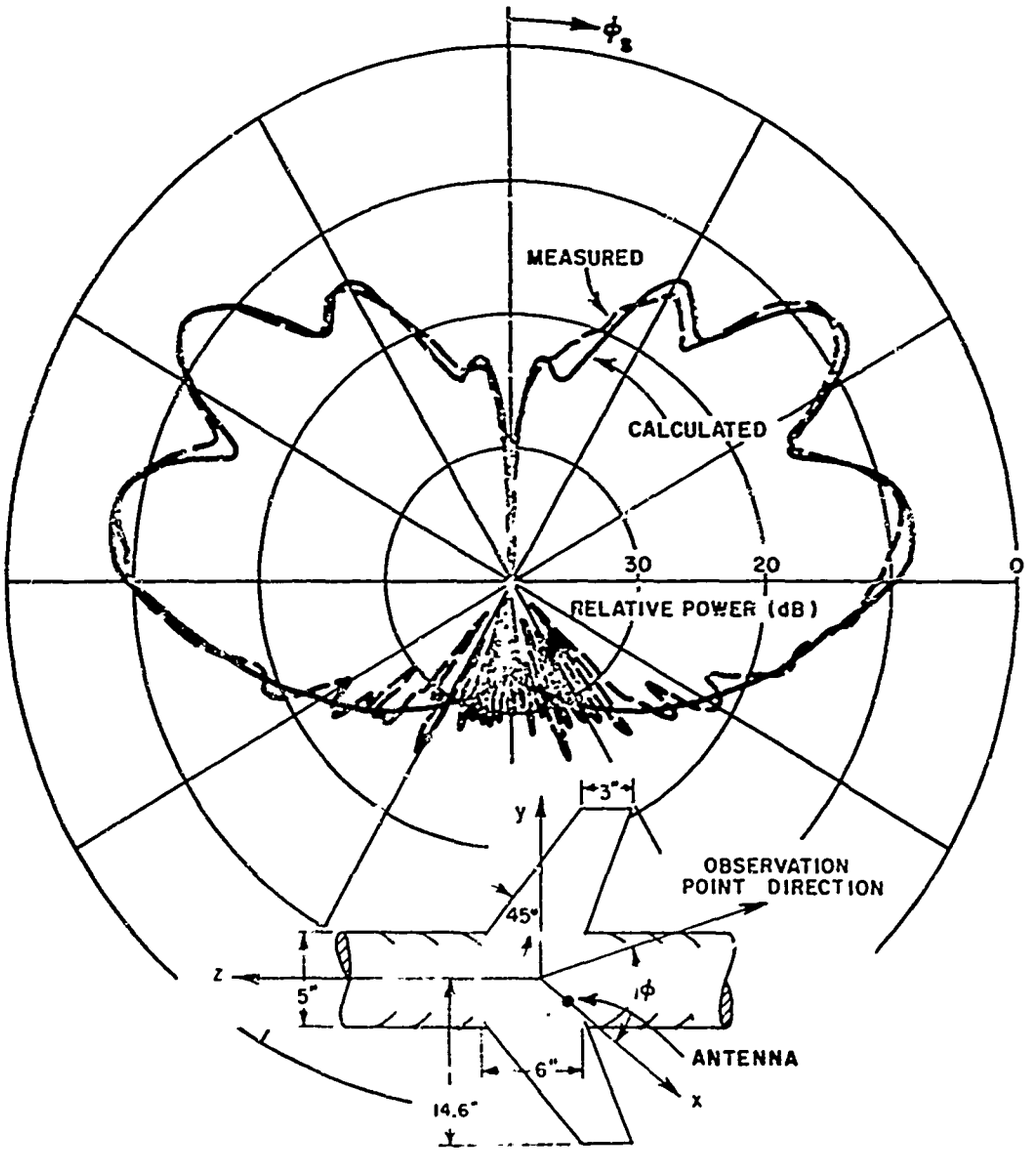

Fig. 6a. Roll plane pattern (E_ϕ) of monopole at point (a_f, $\phi' = 0$, $z' = 0$) with wings attached at a 45° position above the center.

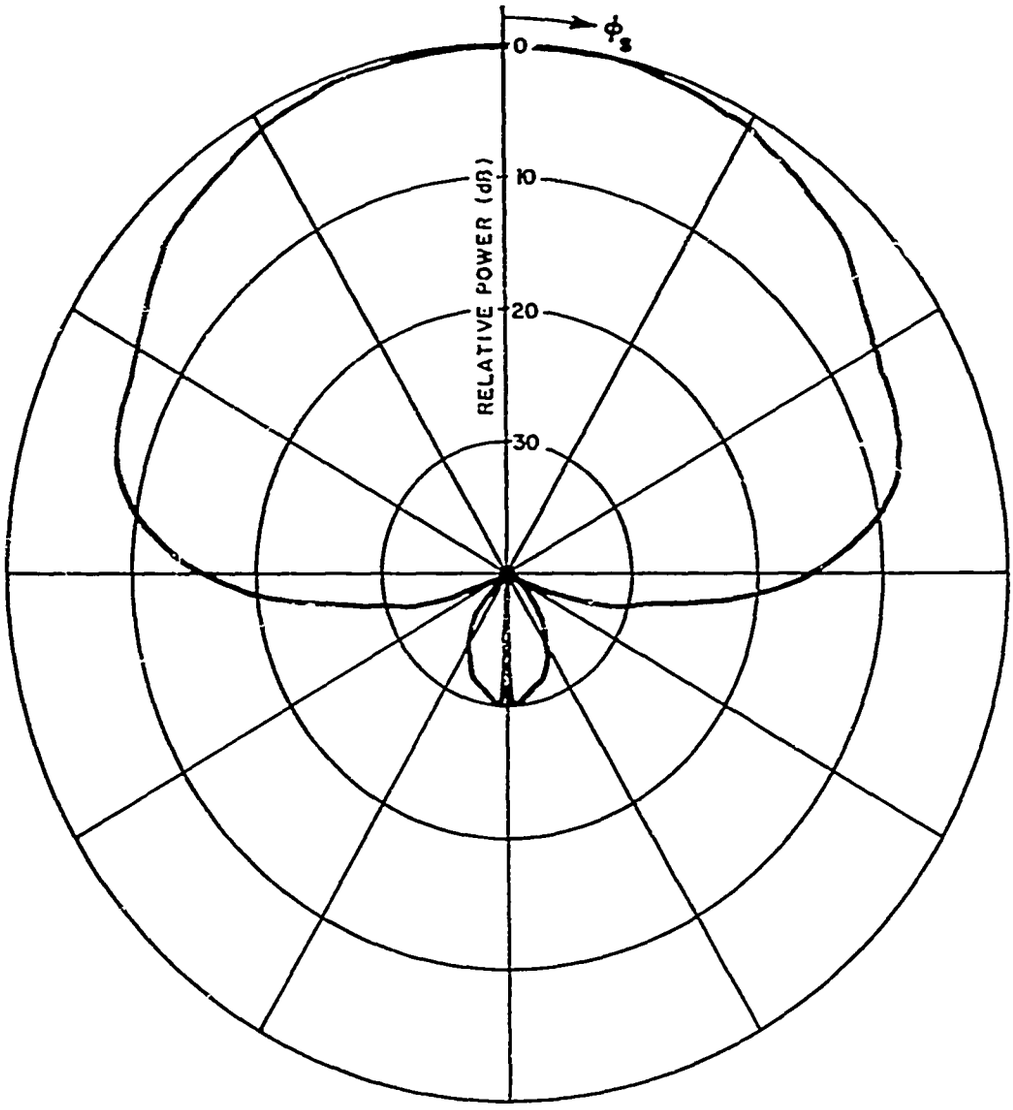

Fig. 6b. Roll plane pattern of circumferential slot (E_θ).

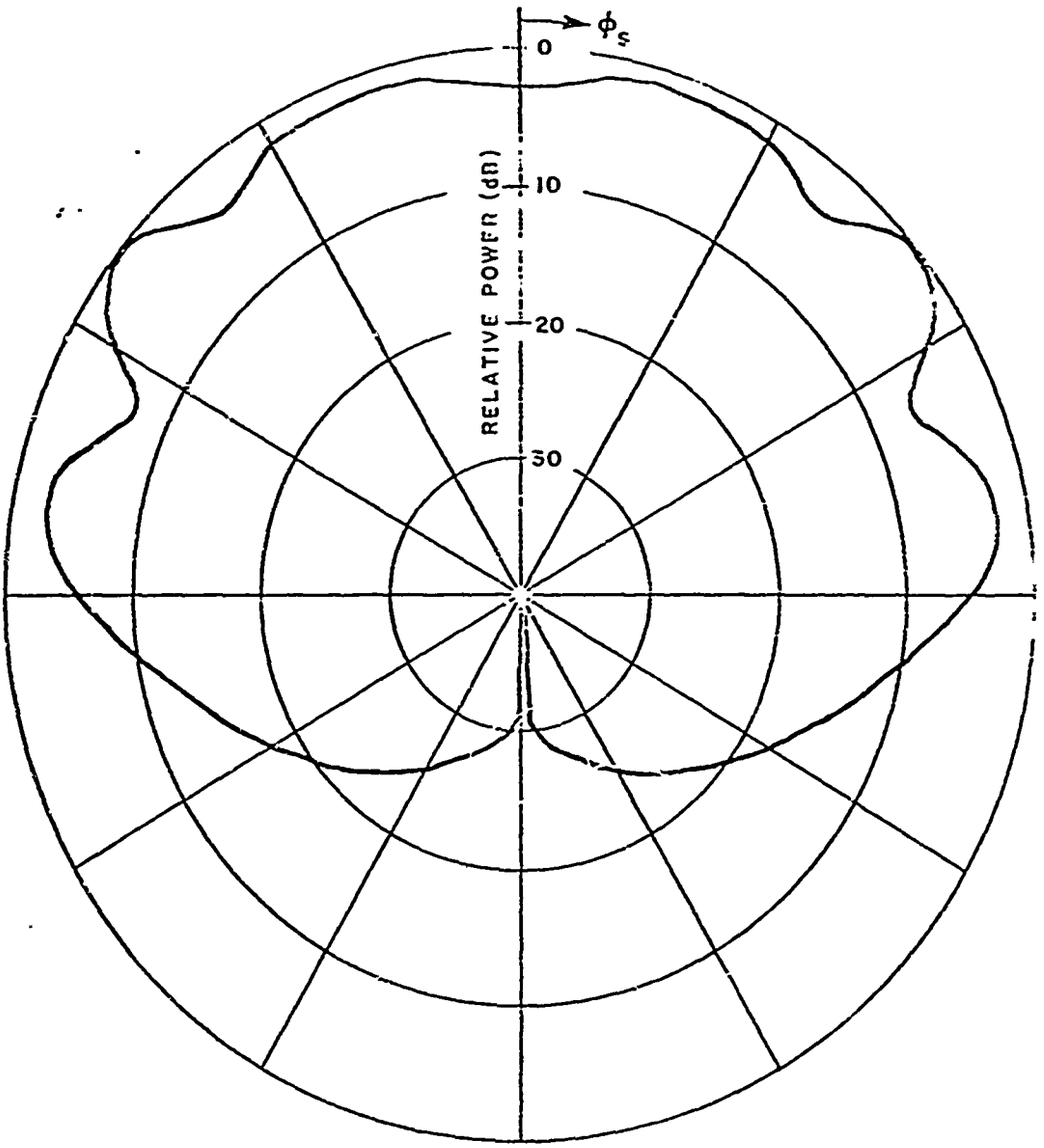

Fig. 6c. Roll plane pattern of axial slot (E_ϕ).

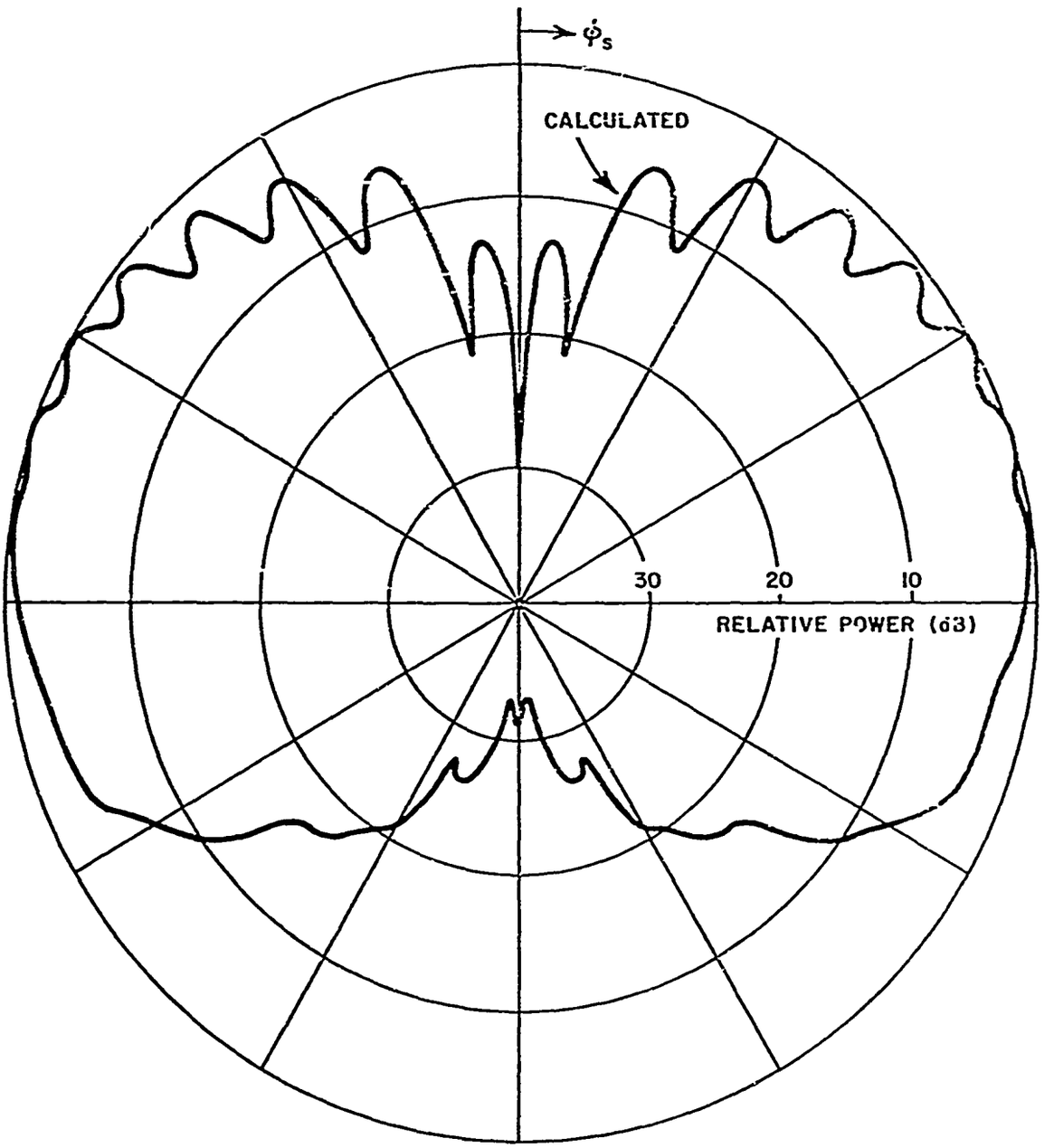

Fig. 7. Roll plane pattern (E_ϕ) of monopole at point (a_f, $\phi' = 0$, $z' = 0$) with the wings attached at 45° position below the center.

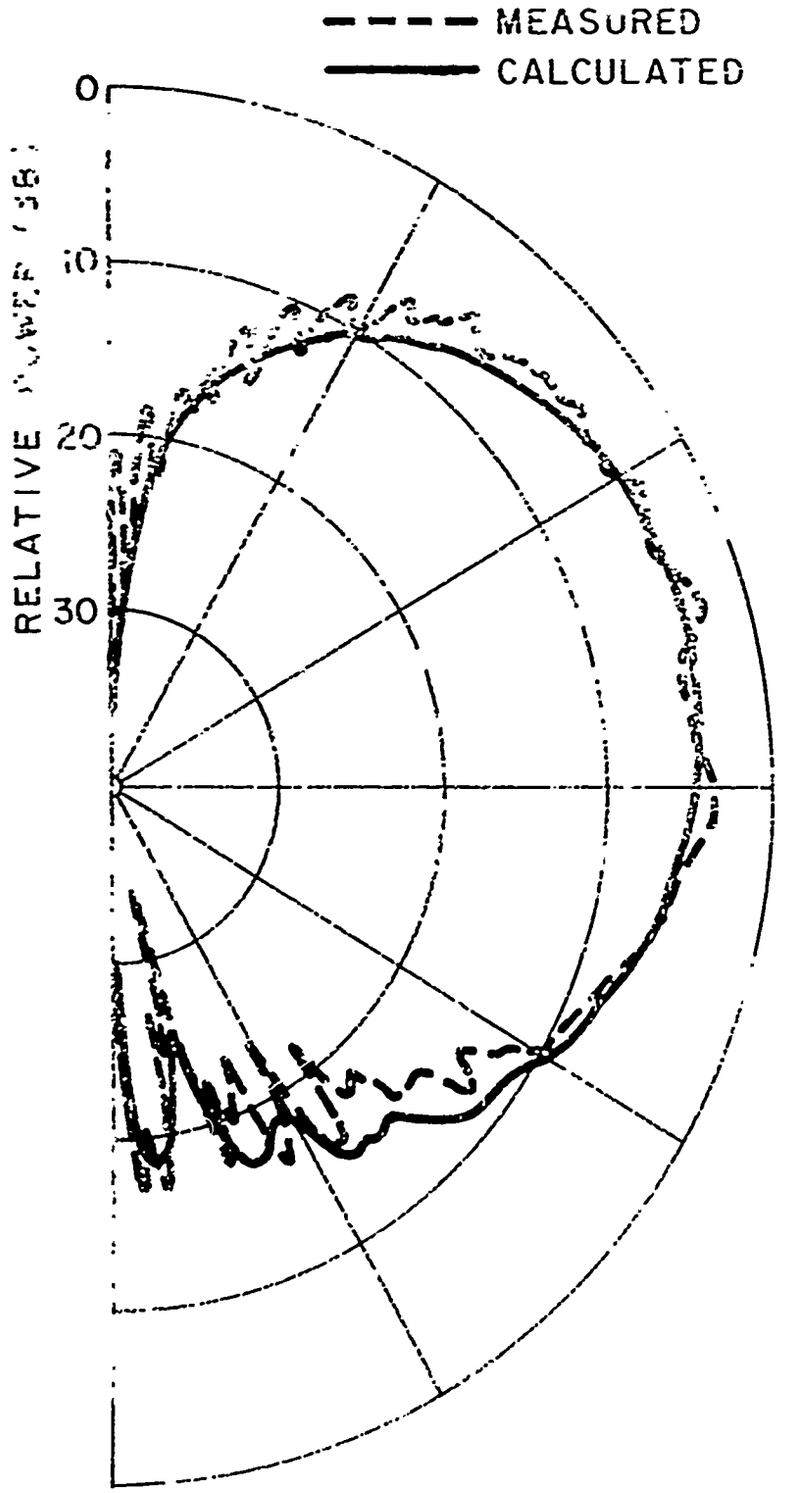

Fig. 8a. Roll plane pattern of a $\lambda/4$ monopole mounted 11" from the nose on the bottom of an 1/8 scale model of an F-4 aircraft.

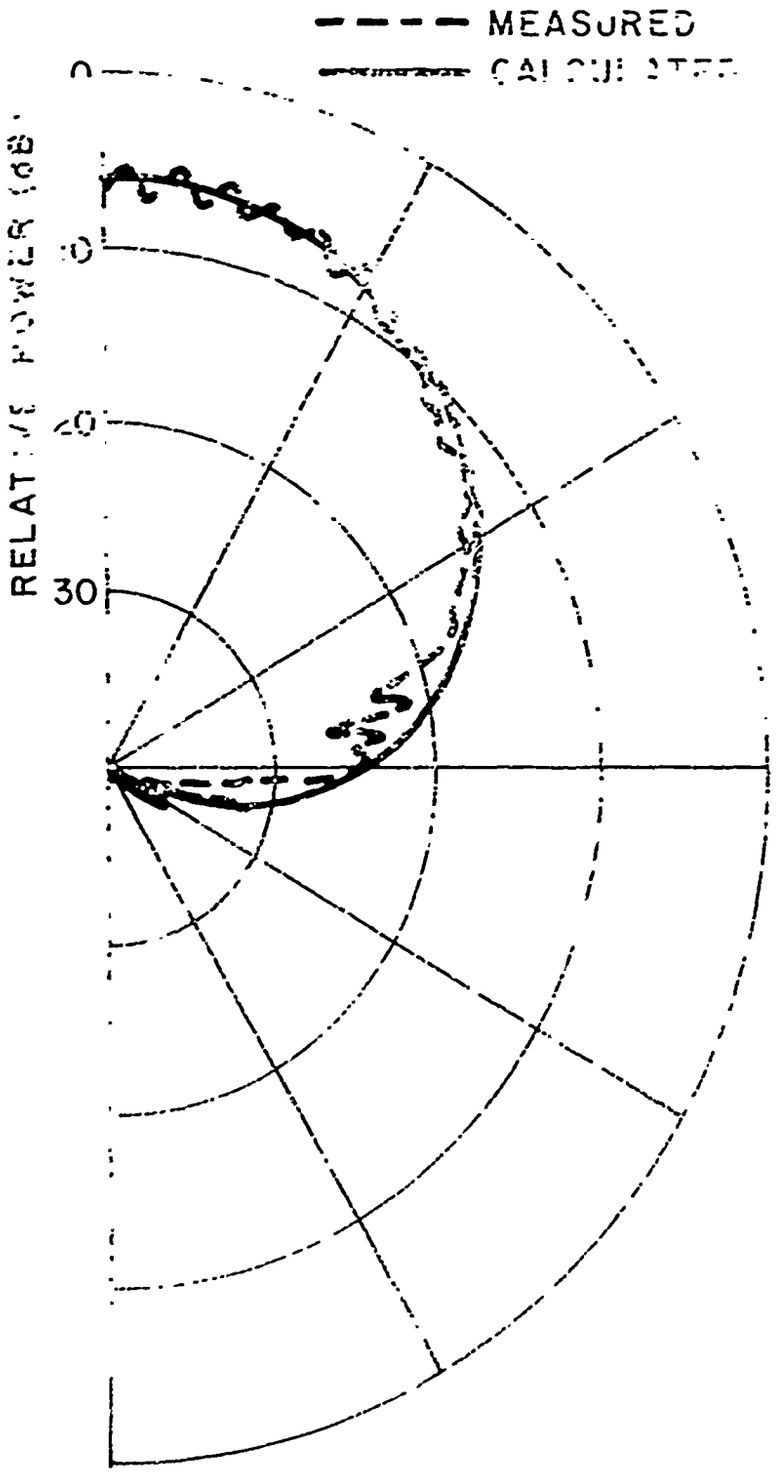

Fig. 8b. Roll plane pattern of a circumferential slot mounted 35-1/4" from the nose on the top of an 1/8 scale model of an F-4 aircraft.

The original solution was based on a corner-by-corner analysis which is invalid for a concave corner. The present approach, which is illustrated in Fig. 9a, uses a complex variable theorem which states that the $\oint_C d\phi$ around a closed contour is equal to 2- if the point is enclosed and zero otherwise. In our case, the point is simply the intersection point of the image ray with the plane of the flat plate and the contour is the wing edge geometry. Using this approach, one is able to handle an arbitrary wing shape. The calculated pattern for an A-6 aircraft, which has a concave corner wing structure, is shown in Fig. 9b.

In Reference [24] it was shown that the engines had very little effect in the azimuth plane (y-z plane in Fig. 1) if the antennas were located near the top or bottom of the fuselage. That solution was developed by first treating the near zone scattered fields from a finite cylinder. Once that solution was developed and verified it was adapted to the aircraft model simply by adjusting the incident field. The fuselage was again approximated by an infinitely-long circular cylinder. Several examples of this solution are illustrated in Fig. 10.

More recently the effect of the wing in the azimuth plane has been of interest. To solve this problem one can simply apply the previously developed three-dimensional roll plane model and solve now for the field in the azimuth plane instead. Some results of this study are illustrated in Fig. 11. Note that in each case the wings have very little effect. Consequently, for an antenna mounted on the top or bottom of a fuselage, azimuth pattern is mainly affected by the fuselage with only secondary scattering from the wings and engines.

The two-dimensional elevation plane study (x-z plane in Fig. ") was completed under the previous contract, and the solutions presented in Reference [25]. Note that our most general solution is a section-matching GTD solution which can handle an arbitrary convex fuselage shape. However, this solution can fail in the shadow region especially when the scattered fields are small (less than 20 dB with respect to the main beam level). This results since the three-dimensional effects become significant and, in some cases, even dominant. Thus, in order to improve this elevation plane solution, one must handle the three-dimensional effects which are considered in the next section. On the other hand, one should realize that he can predict when this solution fails by taking the equivalent values from the roll plane solution (θ=90° and ϕ=0° and 180°). If the two-dimensional elevation plane solution is dominant, then the three-dimensional effects must be secondary and can be neglected in the elevation plane. One can use a similar approach to determine if the three-dimensional effects are significant in the roll plane.

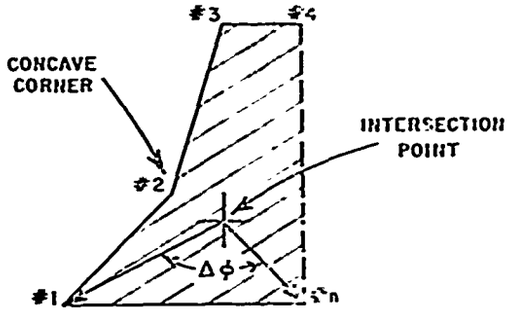

Fig. 9a. Intersection point geometry for plate with concave corner.

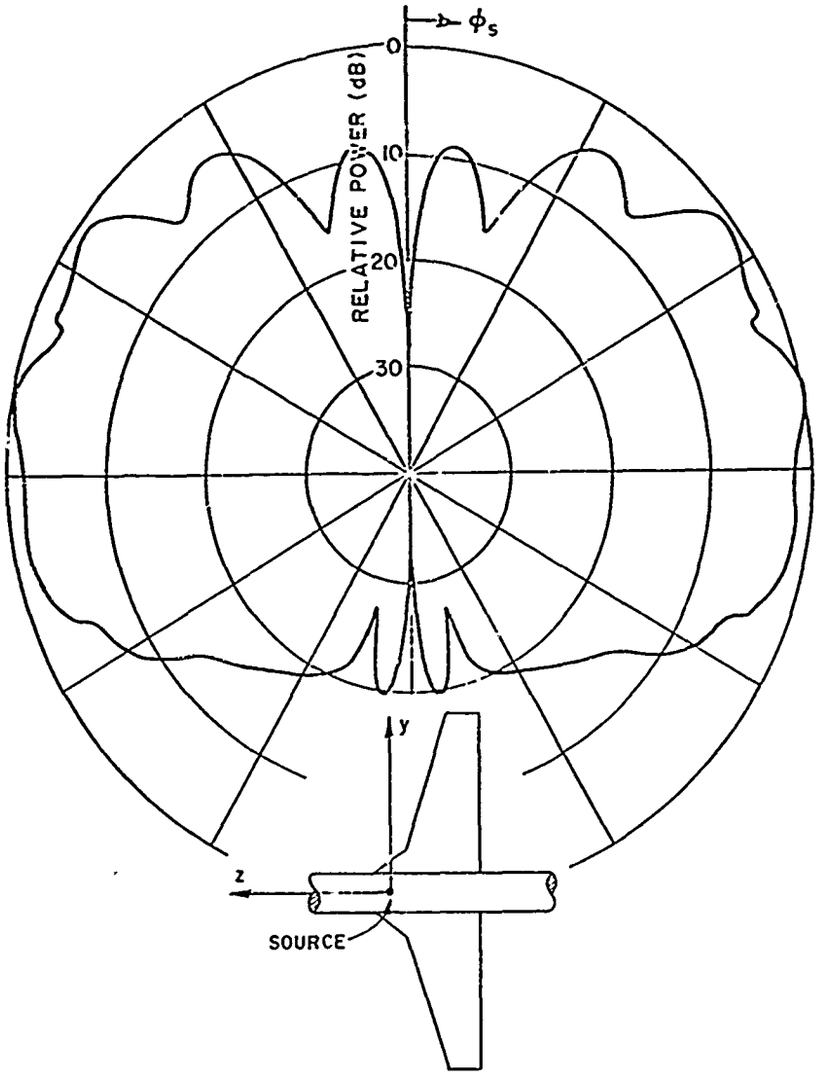

Fig. 9b. Roll plane pattern of λ/4 monopole (E_ϕ) of A-6 aircraft. Frequency = 0.54 GHz.

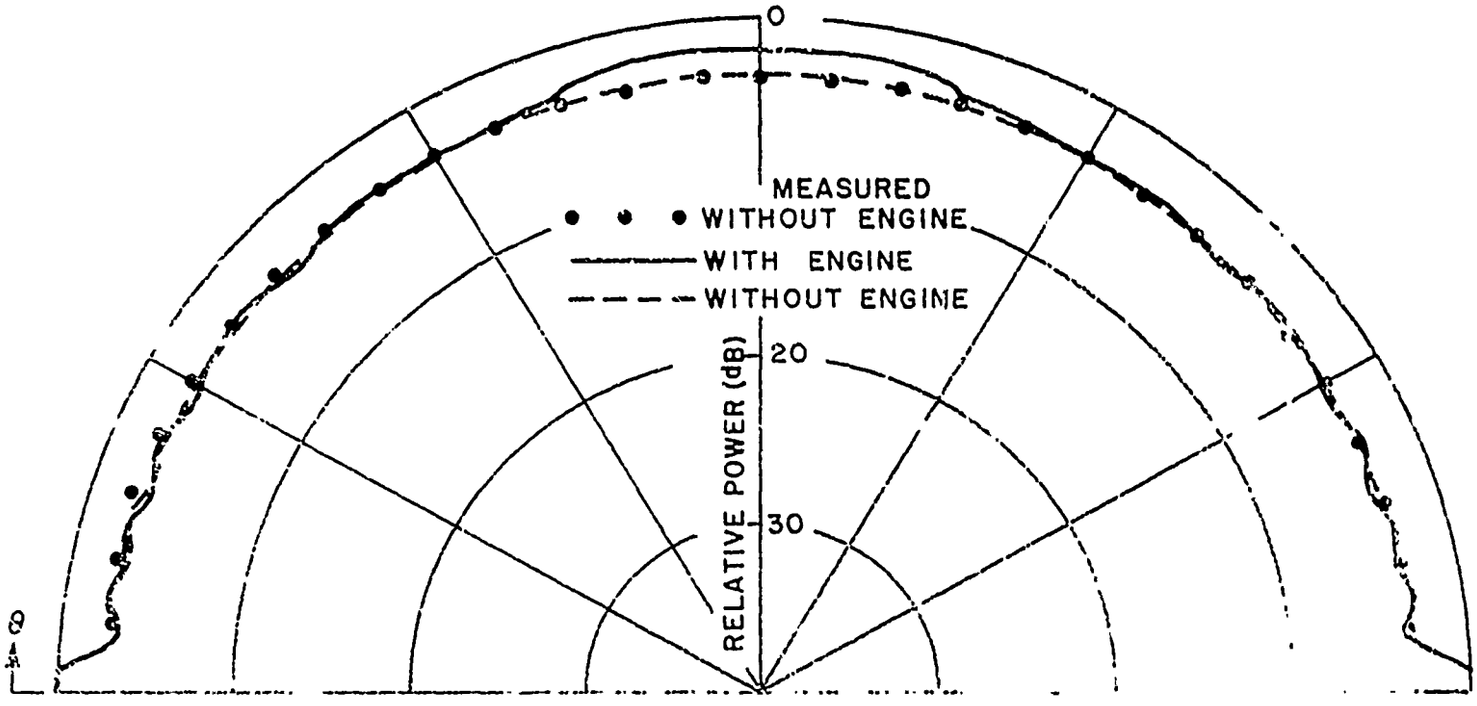

Fig. 10a. Azimuth plane pattern of monopole (E_ϕ) with and without engine.

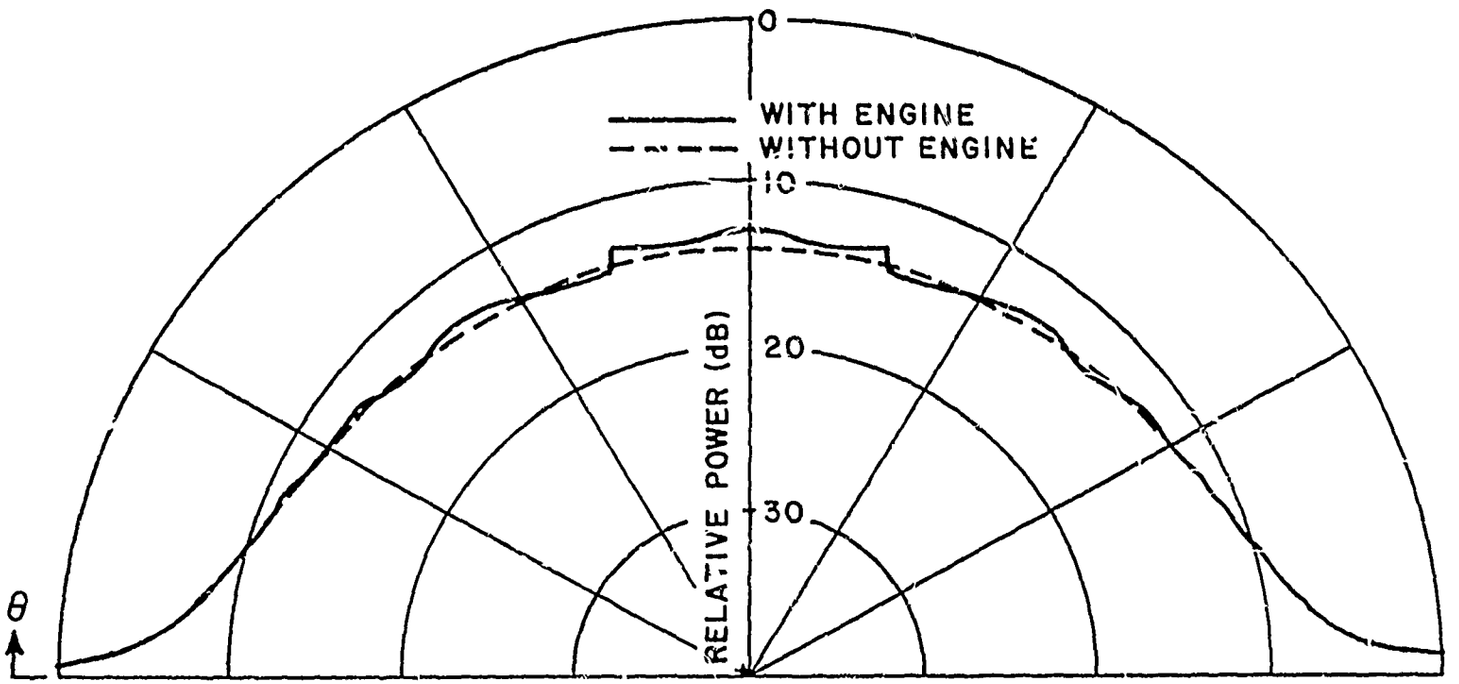

Fig. 10b. Azimuth plane pattern of circumferential slot (E_θ) with and without engine.

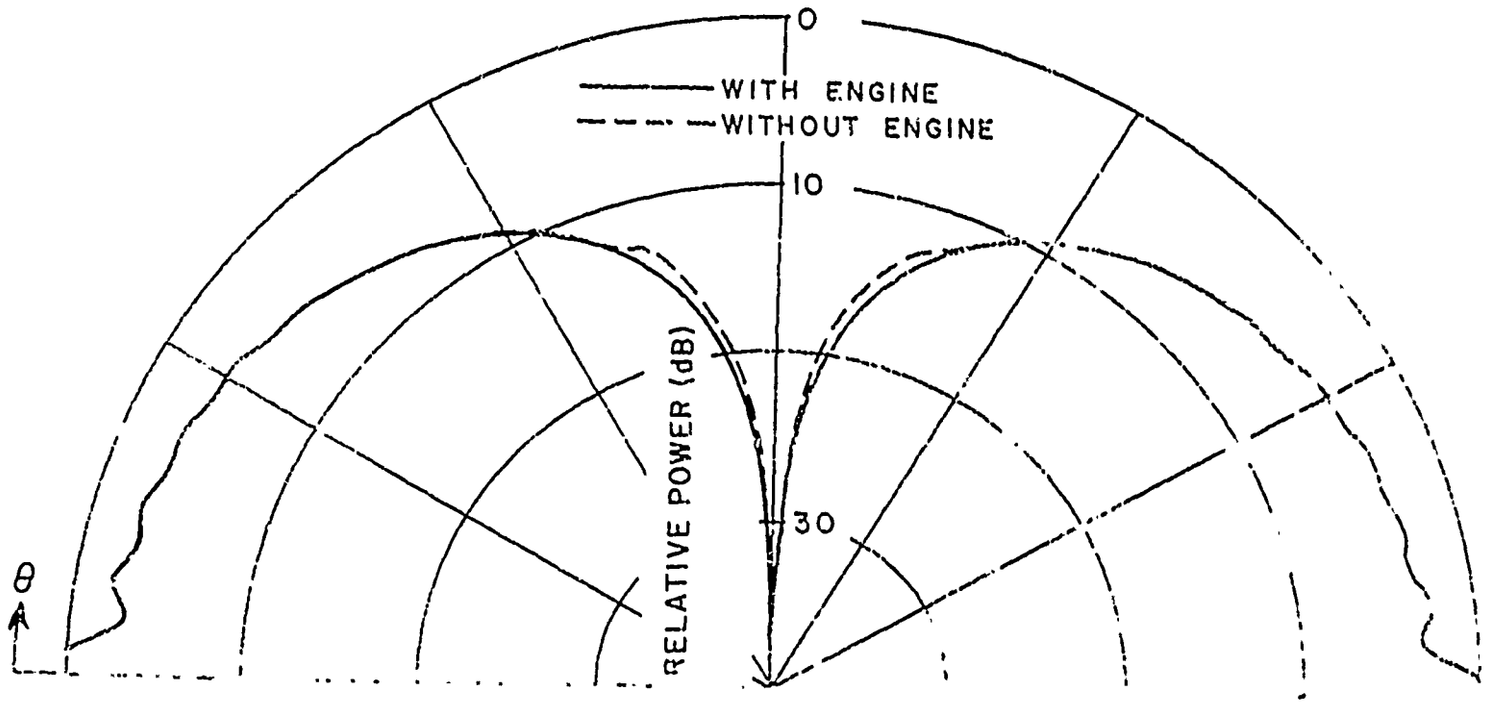

Fig. 10c. Azimuth plane pattern of circumferential slot (E_ϕ) with and without engine.

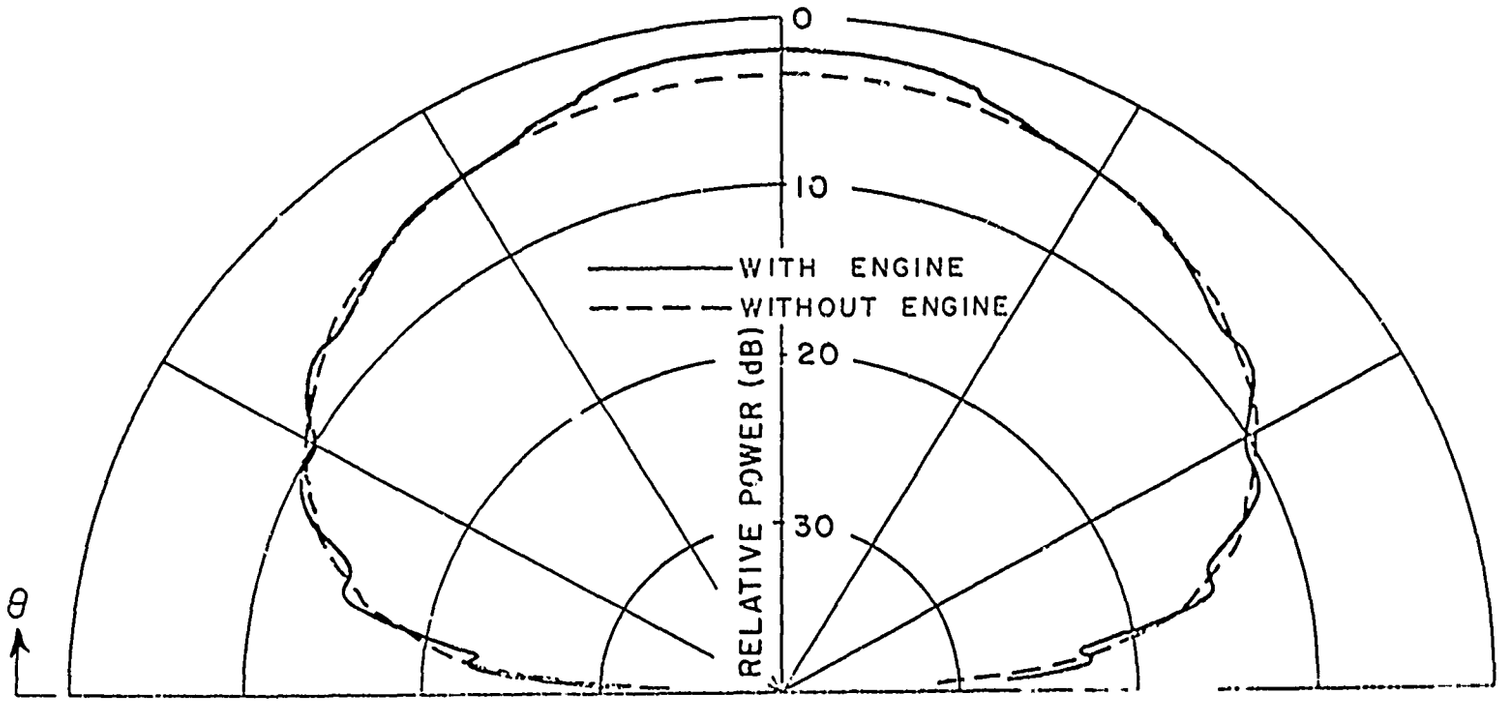

Fig. 10d. Azimuth plane pattern of axial slot (E_ϕ) with and without engine.

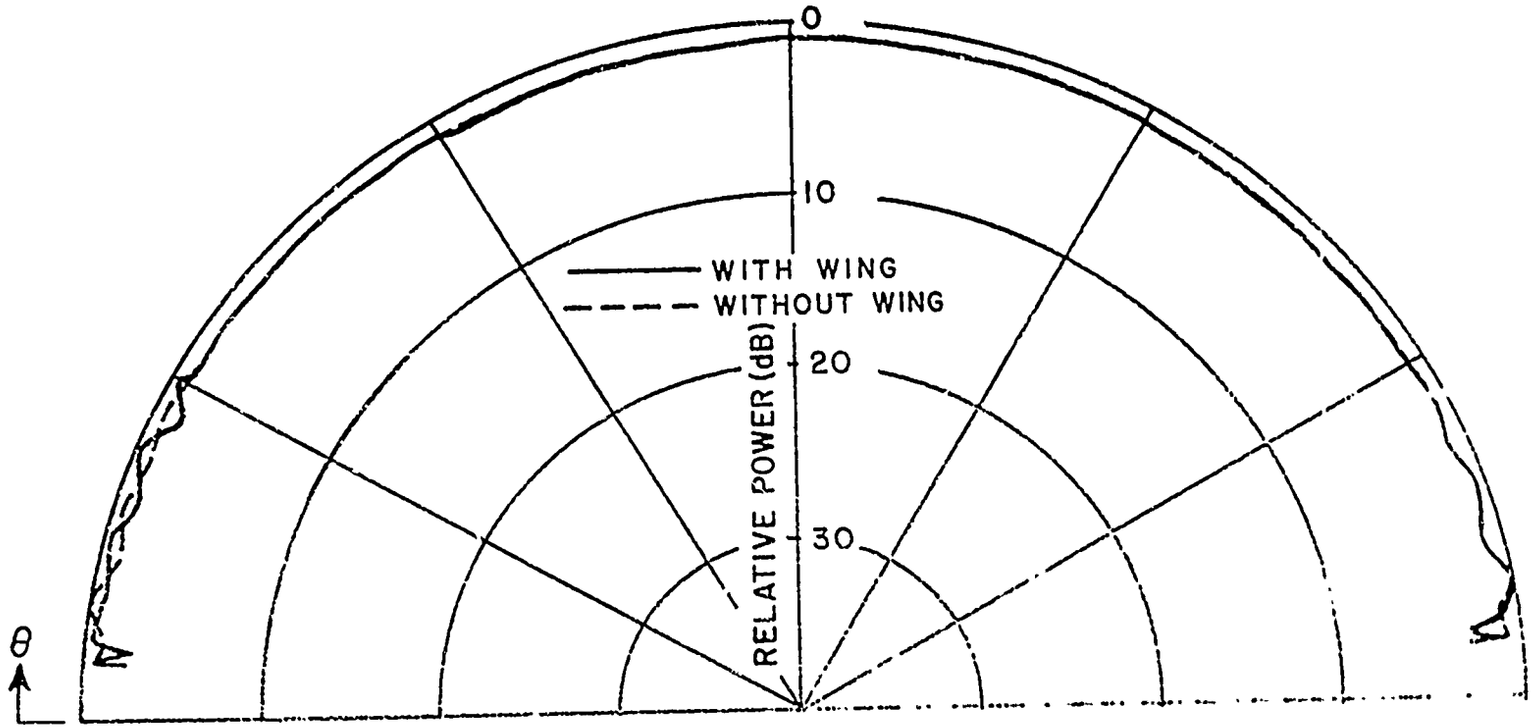

Fig. 11a. Azimuth plane pattern of monopole (E_ϕ) with and without wing.

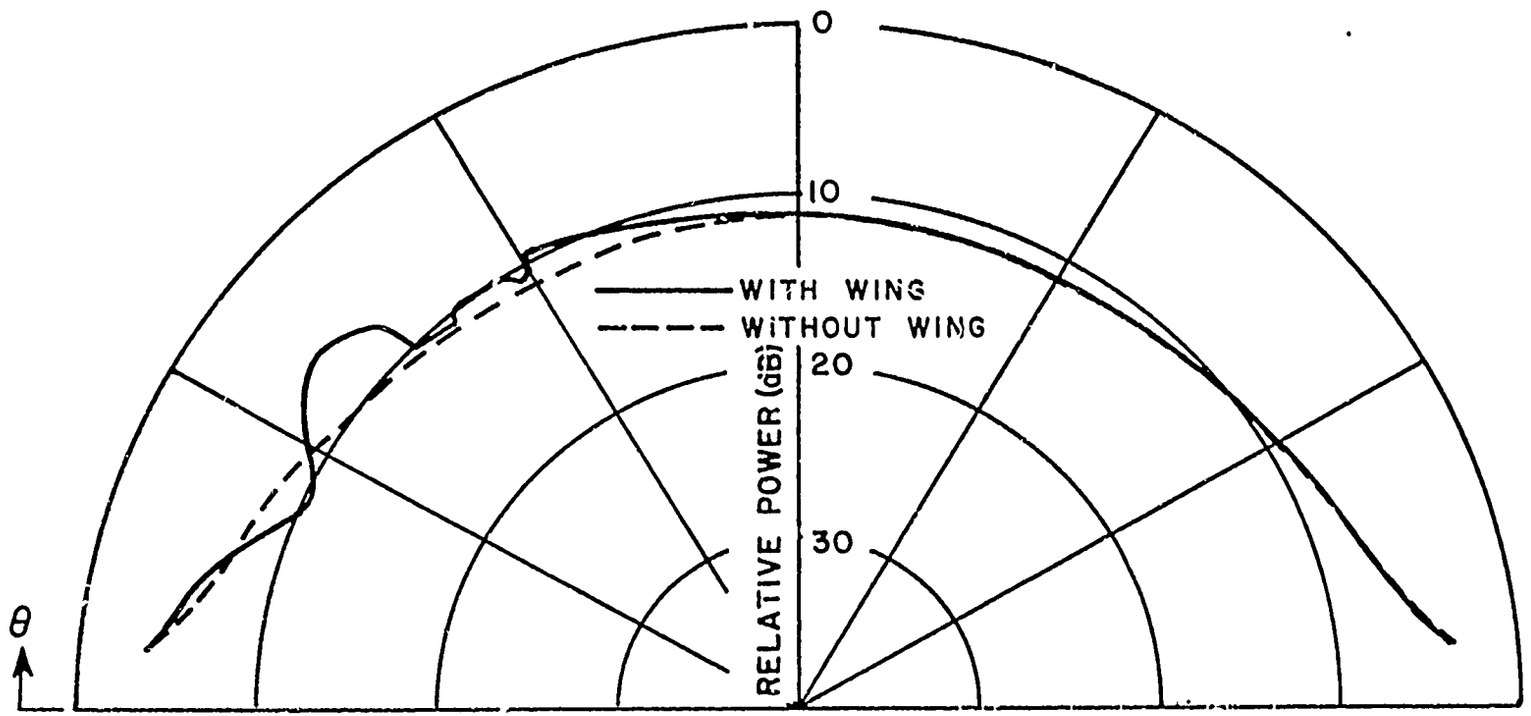

Fig. 11b. Azimuth plane pattern of circumferential slot (E_θ) with and without wing.

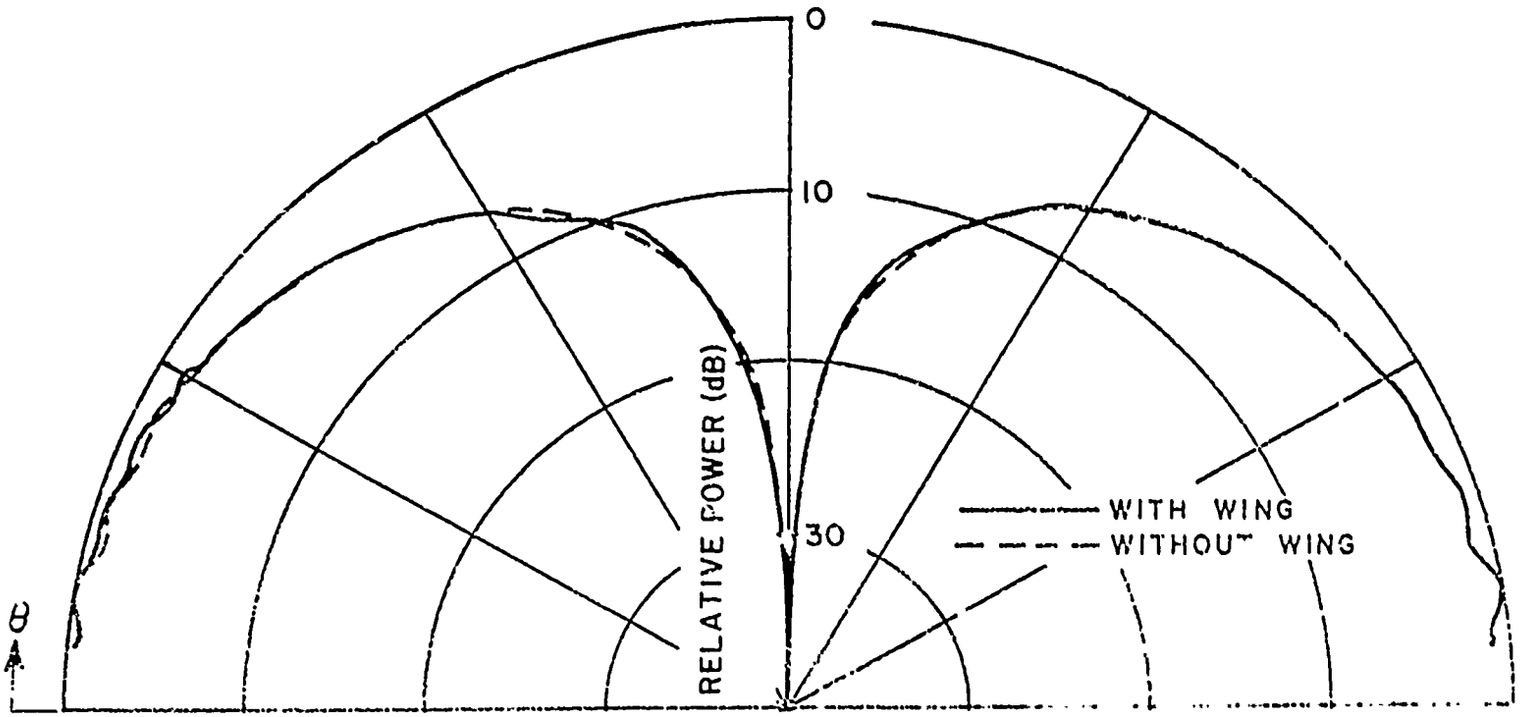

Fig. 11c. Azimuth plane pattern of circumferential slot (E_ϕ) with and without wing.

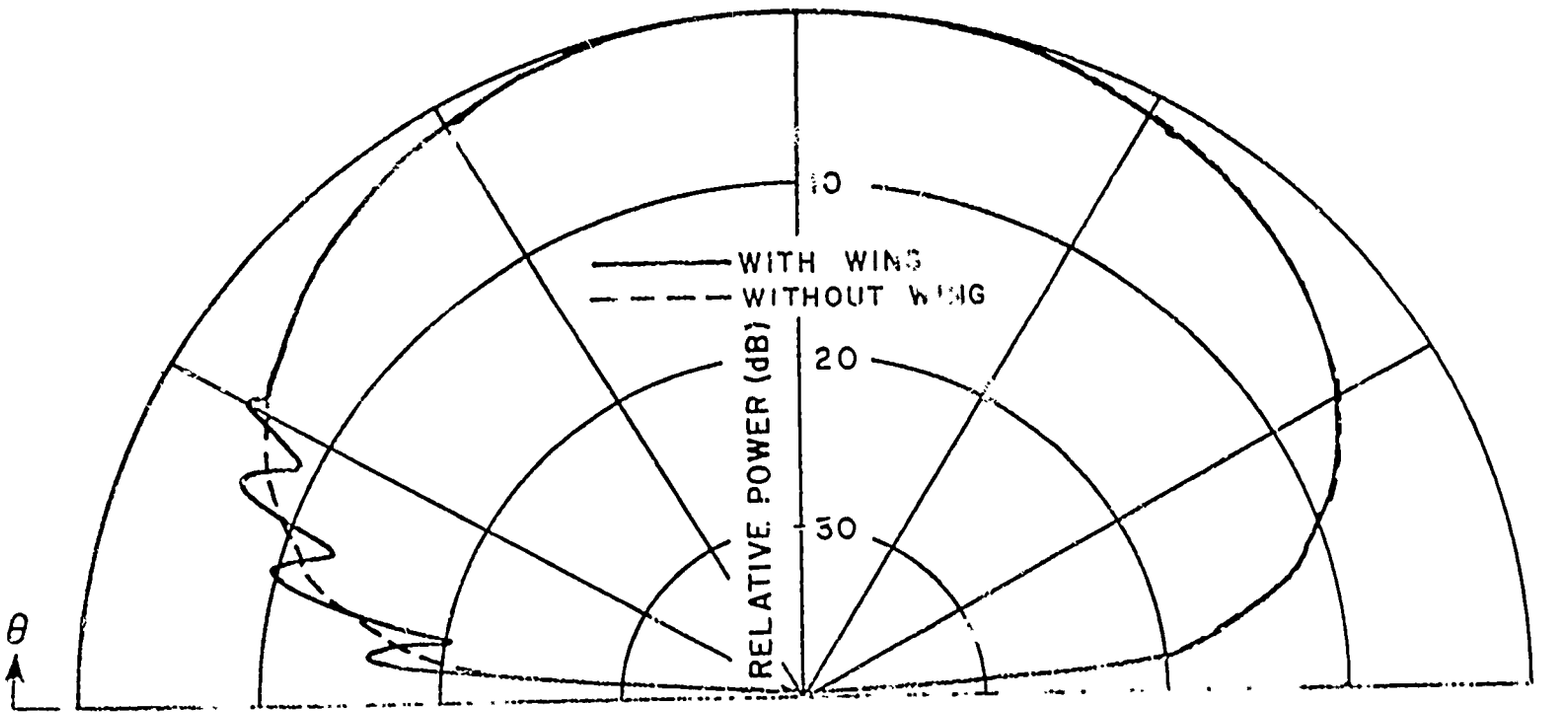

Fig. 11d. Azimuth plane pattern of axial slot (E_ϕ) with and without wing.

III. VOLUMETRIC PATTERN ANALYSIS

As stated earlier, for a source mounted on the fuselage of an arbitrary aircraft near the extreme top or bottom, the fuselage shape has the dominant effect on the resulting antenna pattern. The wings and other flat plate structures can have strong effects in certain sectors of the pattern but they are not as dominant as the fuselage especially when the complete volumetric pattern is considered. For these reasons the volumetric pattern of an antenna mounted on a three-dimensional isolated fuselage must be analyzed. Nevertheless, the wings and various other structures can be added to this solution in the future as was done in the roll plane.

Previously, aircraft models were considered that would resemble a wide variety of aircraft shapes and yet could also be analyzed with reasonable accuracy. In this case, it is quite obvious that the three-dimensional nature of the fuselage must be modelled if one is to adequately determine volumetric patterns. In the elevation plane it was found that the longitudinal profile of the fuselage had to be accurately represented. This resulted in the development of the Section-Matching GTD solution in which the profile was described by a finite number of points. In the roll plane, the circular cross-section was found to be adequate. One obvious extension of these observations is to consider a fuselage which is analytically described by a surface of revolution. In this case the profile is again described by a set of points which in turn are revolved about the axis of the fuselage. In this way the important features of our past studies in the three principal planes are incorporated in this new three-dimensional study. Not only is this shape quite versatile but it can also be analyzed by extending the techniques that were developed previously.

The geometry of this problem is illustrated in Fig. 12. Note that the surface is defined by a set of points, which are used to specify $R(\theta)$ for $0 \leq \theta \leq 180°$. For the cases considered here $R(\theta)$ is defined every 0.5° which requires a total of 361 points to define the surface.

As presented in Reference [26] the rays which propagate outward from a source travel around the surface along geodesic paths while energy is continually being diffracted in the tangent direction at each point along the path. Thus, the first step in computing the volumetric pattern of an antenna mounted on a three-dimensional convex body is finding a numerical technique to specify the geodesic paths.

The geodesic differential equations for an arbitrary surface of revolution in the preferred coordinate system, as illustrated in Fig. 12, are developed here using tensor analysis. Any point on this surface is, then, defined by

$$x(\theta,\phi) = R(\theta) \sin\theta \cos\phi$$
$$y(\theta,\phi) = R(\theta) \sin\theta \sin\phi$$
$$z(\theta,\phi) = R(\theta) \cos\theta.$$

The unit tangent vectors on the surface are given by

$$\hat{e}_1(\theta,\phi) = \left[\hat{x}\left(\frac{dR}{d\theta}\sin\theta + R\cos\theta\right)\cos\phi + \hat{y}\left(\frac{dR}{d\theta}\sin\theta + R\cos\theta\right)\sin\phi - \hat{z}\left(\frac{dR}{d\theta}\cos\theta - R\sin\theta\right)\right] \Big/ \sqrt{\left(\frac{dR}{d\theta}\right)^2 + R^2}$$

and

$$\hat{e}_2(\theta,\phi) = -\hat{x}\sin\phi + \hat{y}\cos\phi.$$

The metric tensor is given by

$$g = \begin{pmatrix} \dfrac{\left(\frac{dR}{d\theta}\right)^2 + R^2}{\sqrt{\left(\frac{dR}{d\theta}\right)^2 + R^2\,(1+\sin^2\theta)}} & 0 \\ 0 & \dfrac{R^2\sin^2\theta}{\sqrt{\left(\frac{dR}{d\theta}\right)^2 + R^2\,(1+\sin^2\theta)}} \end{pmatrix}.$$

Using the above information, the Christoffel symbols are given by

$$\Gamma^1_{11} = \frac{\frac{dR}{d\theta}\left(\frac{d^2R}{d\theta^2} + R\right)}{\left(\frac{dR}{d\theta}\right)^2 + R^2}$$

$$\Gamma^1_{22} = \frac{-R\sin\theta\,(R\cos\theta + \frac{dR}{d\theta}\sin\theta)}{\left(\frac{dR}{d\theta}\right)^2 + R^2}$$

$$\Gamma^2_{21} = \Gamma^2_{12} = \frac{R\cos\theta + \frac{dR}{d\theta}\sin\theta}{R\sin\theta}$$

$$\Gamma^1_{12} = \Gamma^1_{21} = \Gamma^2_{11} = \Gamma^2_{22} = 0\ .$$

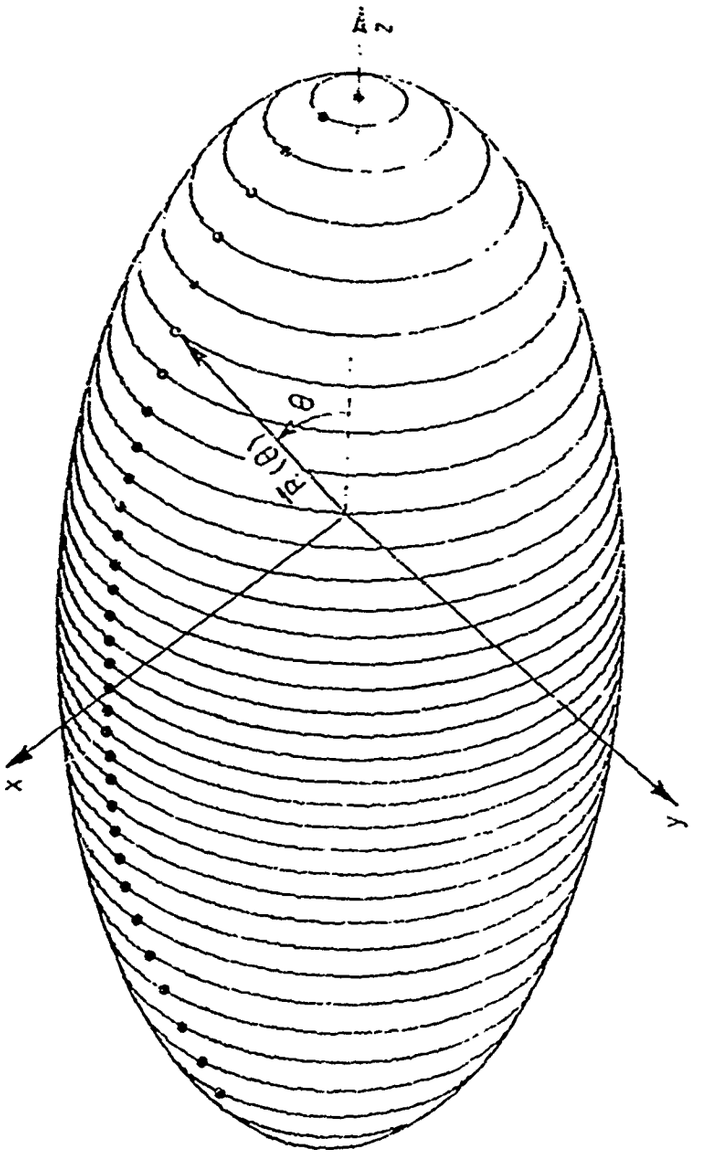

Fig. 12. Surface of revolution described by a finite set of points.

Substituting these results into the geodesic differential equation (Reference [27]), one finds that the geodesic paths are defined by

$$(1) \qquad \frac{d^2\theta}{ds^2} + \Gamma^1_{11}\left(\frac{d\theta}{ds}\right)^2 + 2\,\Gamma^1_{12}\,\frac{d\theta}{ds}\,\frac{d\phi}{ds} + \Gamma^1_{22}\left(\frac{d\phi}{ds}\right)^2 = 0$$

$$(2) \qquad \frac{d^2\phi}{ds^2} + \Gamma^2_{11}\left(\frac{d\theta}{ds}\right)^2 + 2\,\Gamma^2_{12}\,\frac{d\theta}{ds}\,\frac{d\phi}{ds} + \Gamma^2_{22}\left(\frac{d\phi}{ds}\right)^2 = 0$$

where s is the arclength along the geodesic path. Note that these solutions are valid only for a surface of revolution such that the z-axis coincides with the axis of revolution.

The above geodesic solutions are adequate provided θ is not near 0 or 180°. This is seen in terms of Γ^2_{21} and Γ^2_{12} which are singular for these values. Thus, a new solution must be developed to handle these special cases. This is accomplished by defining a new coordinate system such as shown in Fig. 13. This coordinate system requires a general solution for the geodesic equations such as given below:

$$x(\theta,\phi) = R(\theta,\phi)\sin\theta\cos\phi$$
$$y(\theta,\phi) = R(\theta,\phi)\sin\theta\sin\phi$$
$$z(\theta,\phi) = R(\theta,\phi)\cos\theta$$

$$\Gamma^2_{21} = \Gamma^2_{12} = \frac{R}{G}\left\{\sin\theta\left[\left(\frac{\partial R}{\partial\theta}\right)^2 + R^2\right]\left(\frac{\partial R}{\partial\theta}\sin\theta + R\cos\theta\right) + \frac{dR}{d\phi}\left(R\,\frac{\partial^2 R}{\partial\theta\partial\phi} - \frac{\partial R}{\partial\theta}\,\frac{\partial R}{\partial\phi}\right)\right\}$$

$$\Gamma^2_{22} = \frac{\left(R\,\frac{dR}{\partial\phi}\right)}{G}\left\{\sin^2\theta\left[R^2 + 2\left(\frac{\partial R}{\partial\theta}\right)^2\right] + R\left[\frac{\partial^2 R}{\partial\phi^2} + \sin\theta\cos\theta\,\frac{\partial R}{\partial\theta}\right]\right\}$$

$$\Gamma^2_{11} = \frac{\left(R\,\frac{\partial R}{\partial\phi}\right)}{G}\left[R\,\frac{\partial^2 R}{\partial\theta^2} - 2\left(\frac{\partial R}{\partial\theta}\right)^2 - R^2\right]$$

$$\Gamma^1_{11} = \frac{R}{G}\left(\frac{\partial R}{\partial\theta}\right)\left[R\sin^2\theta\left(R + \frac{\partial^2 R}{\partial\theta^2}\right) + 2\left(\frac{\partial R}{\partial\phi}\right)^2\right]$$

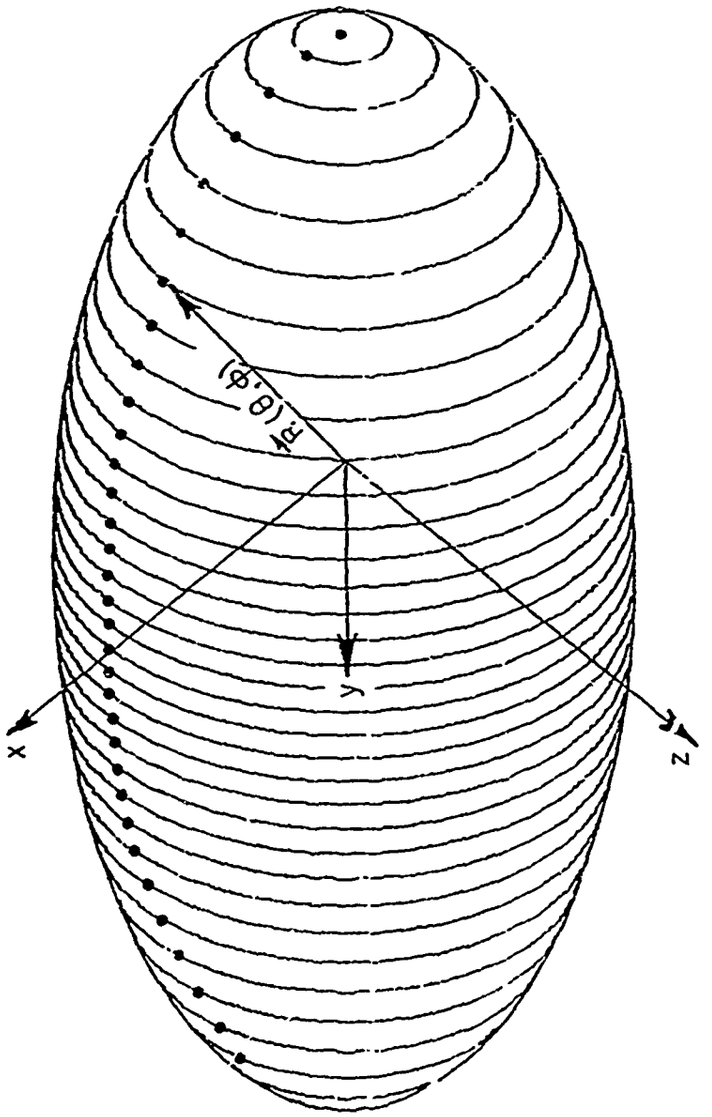

Fig. 13. Surface of revolution described by a general coordinate system.

$$\Gamma^1_{12} = \Gamma^1_{21} = \frac{R}{G}\left\{\sin^2\theta\left[R\frac{\partial R}{\partial\theta}\frac{\partial^2 R}{\partial\phi\partial\theta} + R^2\frac{\partial R}{\partial\phi} - \frac{\partial R}{\partial\phi}\left(\frac{\partial R}{\partial\theta}\right)^2\right] + \frac{\partial R}{\partial\phi}\left[\left(\frac{\partial R}{\partial\phi}\right)^2 - R\frac{\partial R}{\partial\theta}\sin\theta\cos\theta\right]\right\}$$

$$\Gamma^1_{22} = \frac{R\sin\theta}{G}\left\{\left(\sin\theta\frac{\partial R}{\partial\theta}\right)\left[R\frac{\partial^2 R}{\partial\phi^2} - \left(\frac{\partial R}{\partial\phi}\right)^2\right] - \left[\sin\theta\frac{\partial R}{\partial\theta} + R\cos\theta\right]\left[\left(\frac{\partial R}{\partial\phi}\right)^2 + R^2\sin^2\theta\right]\right\}$$

$$G = \frac{1}{R^2\left[\left(\frac{\partial R}{\partial\phi}\right)^2 + \left(\frac{\partial R}{\partial\theta}\right)^2\sin^2\theta + R^2\sin^2\theta\right]}$$

Substituting these results into Eqs. (1) and (2), one has a complete set of geodesic equations for a general surface. This solution is especially important for the elevation plane pattern where $0° \leq \theta \leq 180°$ with $\phi = 0°, 180°$. Obviously, our previous solution could not be applied to solve for this pattern. Some examples of geodesic paths are illustrated in Fig. 14.

Since the antenna is assumed to be mounted on the fuselage of the aircraft, one needs only consider two general types of antennas. These are the monopole type which has a normal electric current moment with respect to the surface and a slot type antenna which has a tangential magnetic current moment. It is assumed that the fields launched by infinitesimal antennas follow the solutions specified for the two-dimensional problem of Reference [28]. Note that in this case the three-dimensional geometry is introduced in terms of the geodesic paths and associated longitudinal and transverse radii of curvature which appear in the diffraction and attenuation coefficients. It is further assumed that the normal and tangential component boundary layer fields propagate around the surface independently. This approximation might be rather poor if the torsion along the geodesic curve varies too greatly; however, this point is not well understood at this time. In any event, the results presented here will be compared with actual measurements to illustrate the validity of these assumptions.

At this time only a convex body is considered in order that the radiation direction can be simply defined by the geodesic tangent direction as was indicated earlier. However, the study of a concave body is an important topic worthy of future consideration.

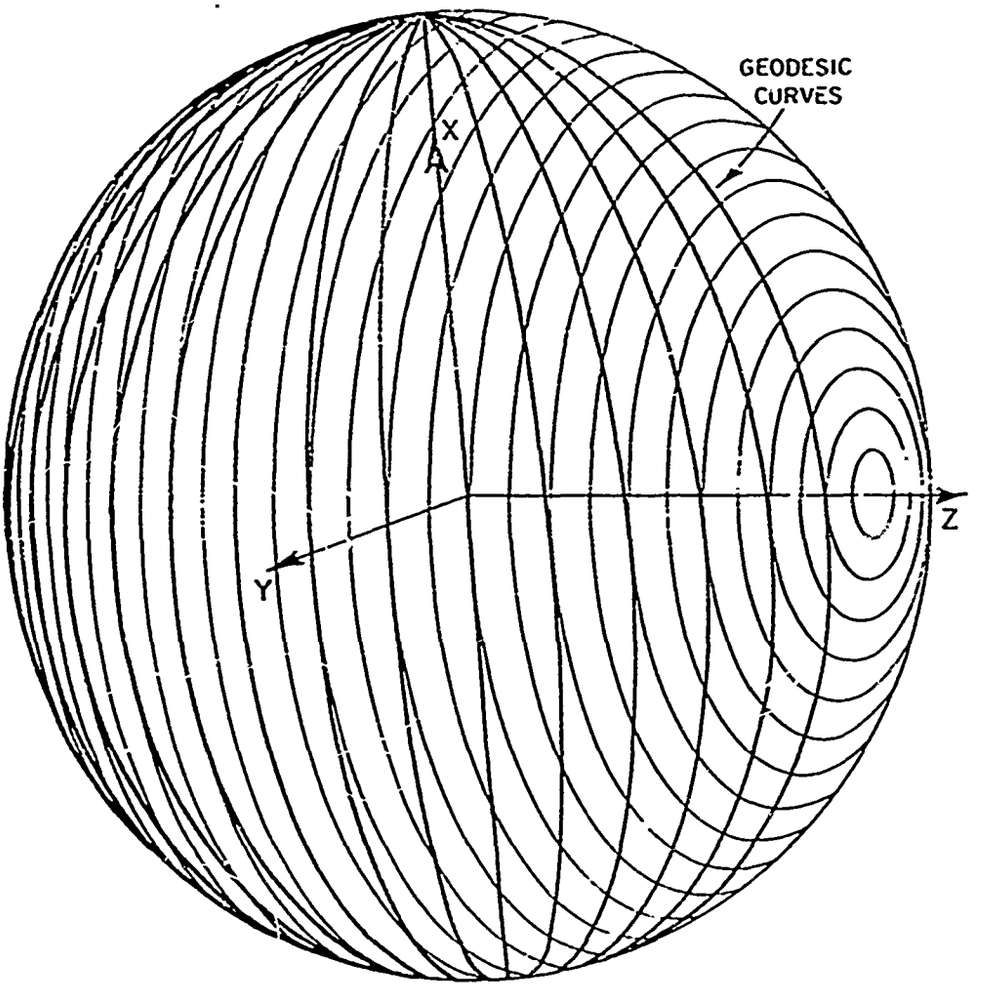

Fig. 14a. Geodesic curves on a sphere with the source at $\vartheta_0 = 90°$, $\phi_0 = 0°$.

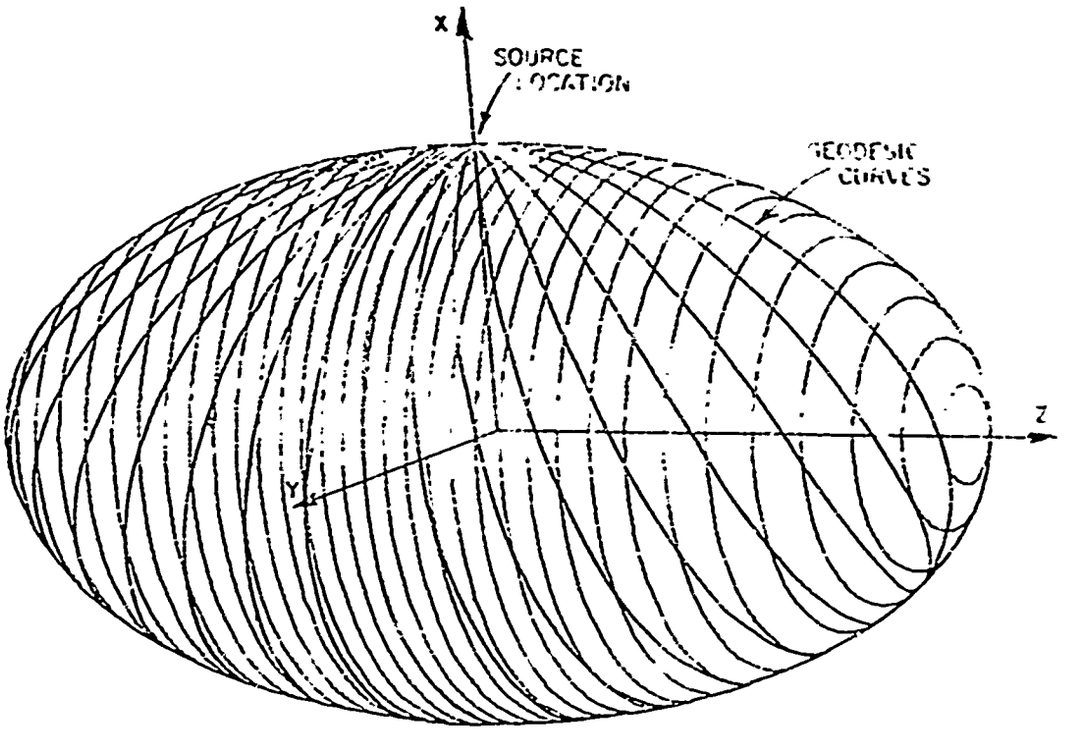

Fig. 14b. Geodesic curves on a 4λ x 2λ prolate spheroid with the source at $\theta_o = 90°$, $\phi_o = 0°$.

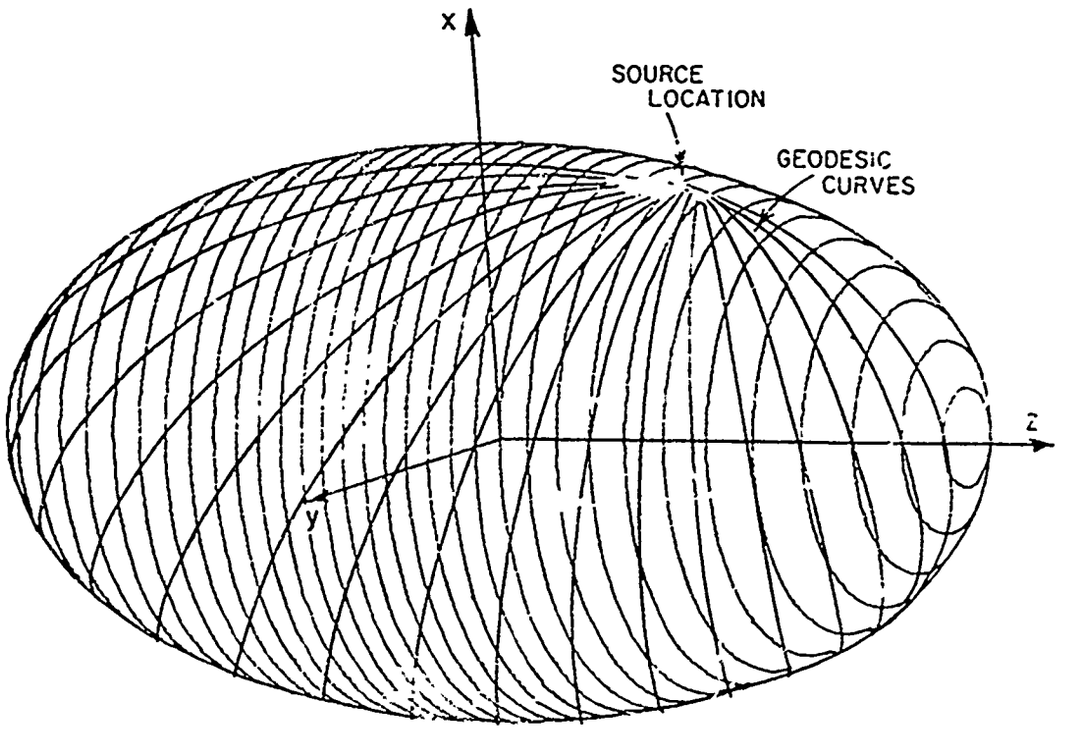

Fig. 14c. Geodesic curves on a 4λ x 2λ prolate spheroid with the source at $\theta_o = 45°$, $\phi_o = 0°$.

Let us first investigate the monopole antenna type whose surface rays propagate outward in all directions from the source with a normal component E-field (or follow the hard boundary condition).

In order to obtain measured patterns off the principal planes using a conventional pattern range, which only revolves about a vertical axis, the body is first rotated by an angle (ξ) as shown in Fig. 15.

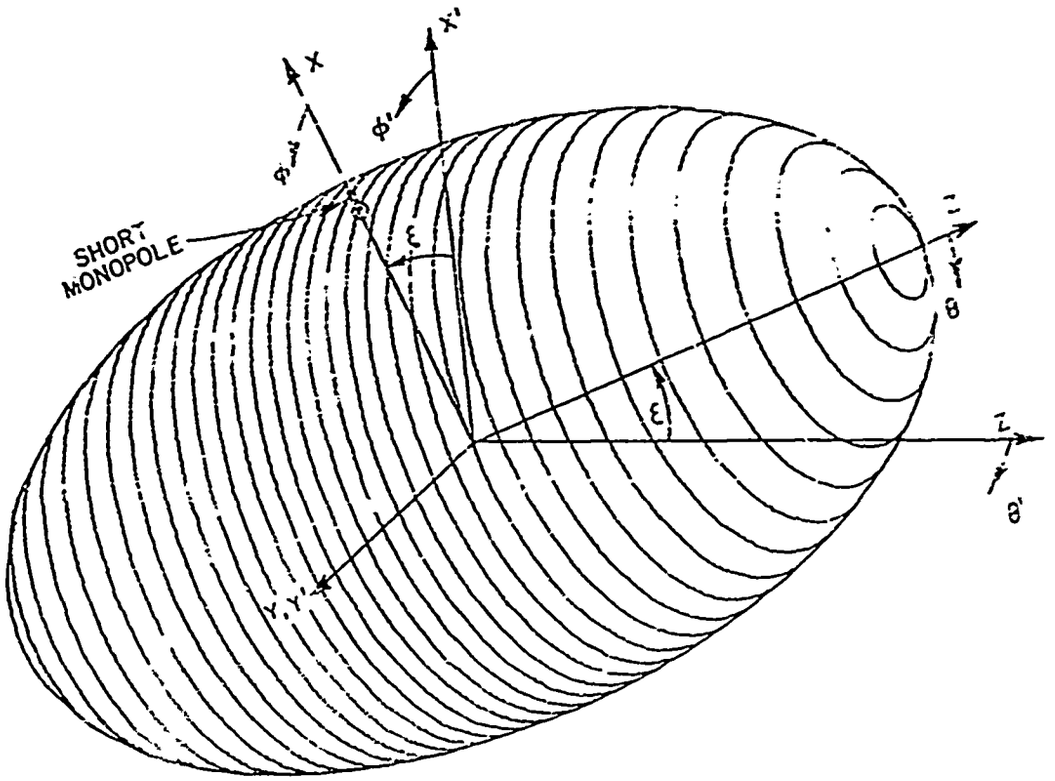

Fig. 15. Rotation of convex surface in order to obtain off-principal plane patterns.

Thus as the body turns about the z'-axis, one obtains the $\hat{\theta}'$ and $\hat{\phi}'$ components of the radiated field. In Fig. 16 the $\hat{\phi}'$-component of the field is illustrated with $\xi = 0°$ for a short monopole mounted on a $4\lambda \times 2\lambda$ prolate spheroid. For this principal plane pattern the comparison between the measured and calculated results is quite good.

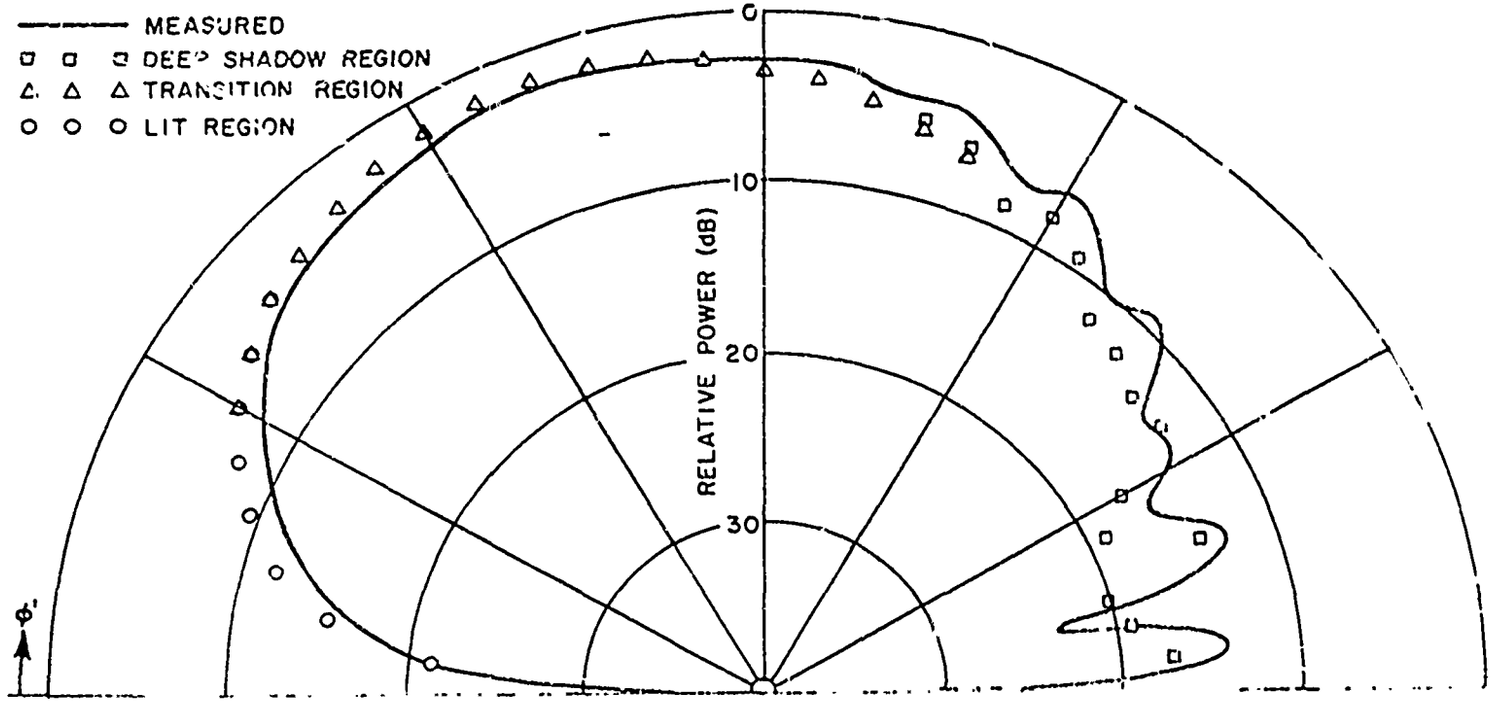

Fig. 16. Principal plane pattern of monopole (E_{ϕ}) with ϕ=0°.

The $\hat{\theta}'$ and $\hat{\phi}'$ components of the radiated field for the same body are illustrated in Figs. 17 and 18 for $\xi = 20°$ and $40°$, respectively. In these off-principal planes the agreement between the results is again quite good.

Even though the problems considered above seem to be rather special cases of the more general problem originally treated at the outset, the results are encouraging especially for the off-principal plane cases. They do tend to verify this approach and the associated approximations at least for the monopole cases considered.

The next case to be considered is that of an arbitrarily oriented slot mounted on a convex surface of revolution. It was shown in Reference [28] that for the two-dimensional problem with the slot mounted parallel (orthogonal) to the cylinder axis that the slot radiated according to the hard (soft) boundary condition in the principal plane. If an arbitrary orientation of the slot were considered then one could assume that the pattern is given in the principal plane by

$$\vec{E} = \vec{E}_{soft} \sin \beta + \vec{E}_{hard} \cos \beta$$

using the geometry illustrated in Fig. 19. Thus, for a slot antenna mounted arbitrarily on a three-dimensional surface with a volumetric pattern desired one can extend this approach by considering that the boundary layer field has a tangential component given by

$$\vec{E}_{tang} = \vec{E}_{soft} \cos(\gamma-\beta) = E_{soft} \cos(\gamma-\beta)\hat{b}$$

and a normal component given by

$$\vec{E}_{normal} = \vec{E}_{hard} \sin(\gamma-\beta) = E_{hard} \sin(\gamma-\beta)\hat{n}$$

where γ is the starting direction of the geodesic path. Note that the above solutions agree in the principal plane ($\gamma = 90°$). It is then assumed that these two components propagate around the surface independent of one another.

In order to measure the pattern of a slot antenna, a finite length slot is considered. Actually for our measured patterns an open-ended waveguide is used except the width is cut down to approximately one-tenth of the wavelength. For this antenna one can compute the pattern by numerically integrating the patterns from three infinitesimal slot antennas which approximate the aperture fields as shown in Fig. 19. This approach is described in Reference [29] and successfully applied in Reference [22]. Using this solution the computed principal plane pattern ($\xi = 0°$ in Fig. 15) is compared with

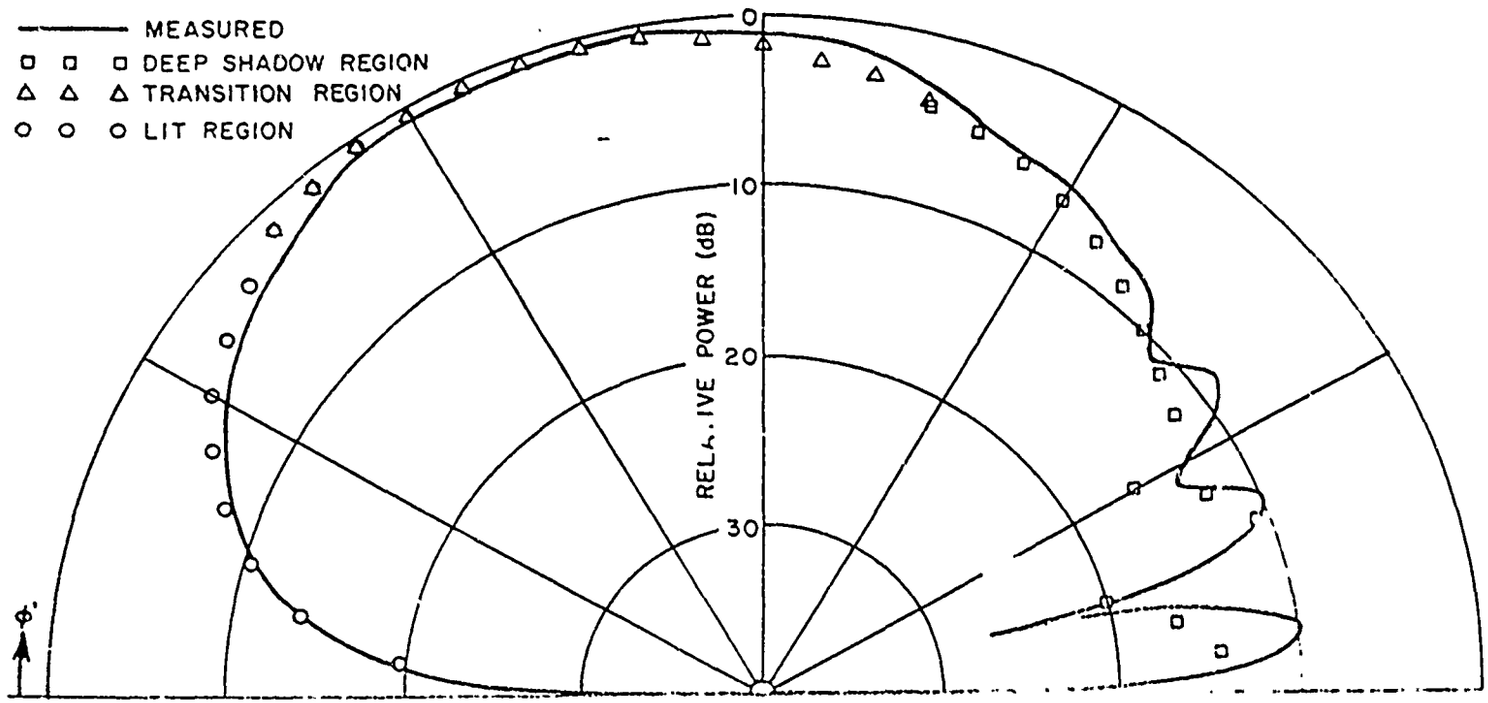

Fig. 17a. Off-principal plane pattern of monopole ($E_{\phi'}$) with ζ=20°.

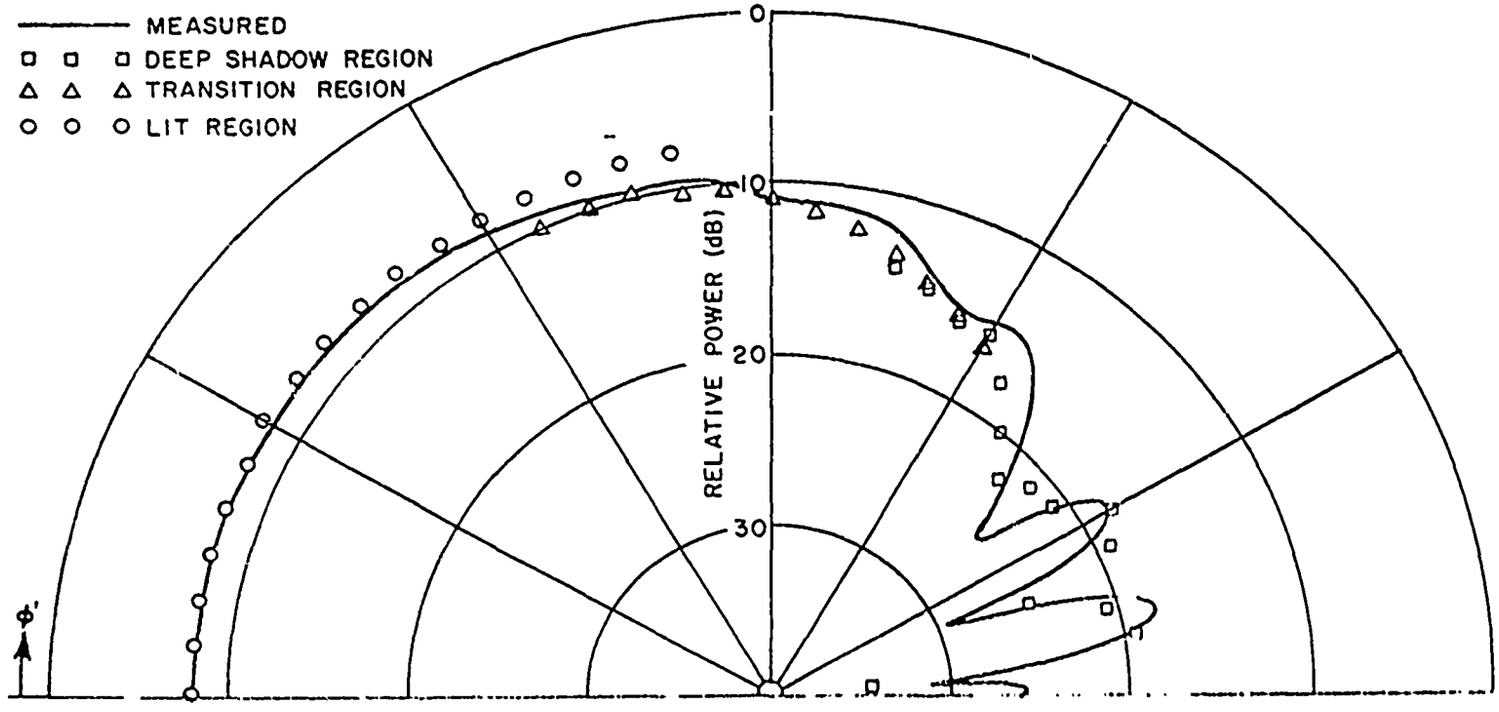

Fig. 17b. Off-principal plane pattern of monopole ($E_{\theta'}$) with ξ=20°.

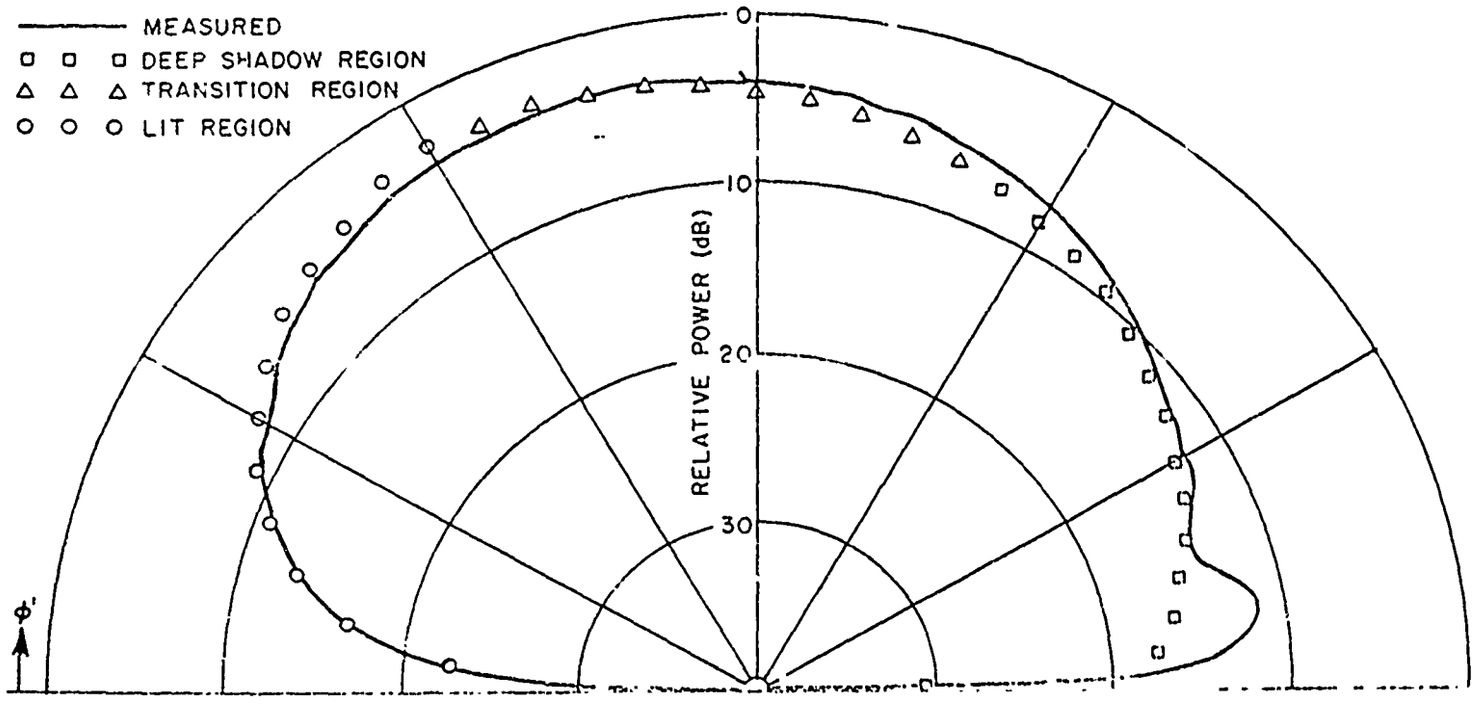

Fig. 18a. Off-principal plane pattern of monopole ($E_{\phi'}$) with ξ=40°.

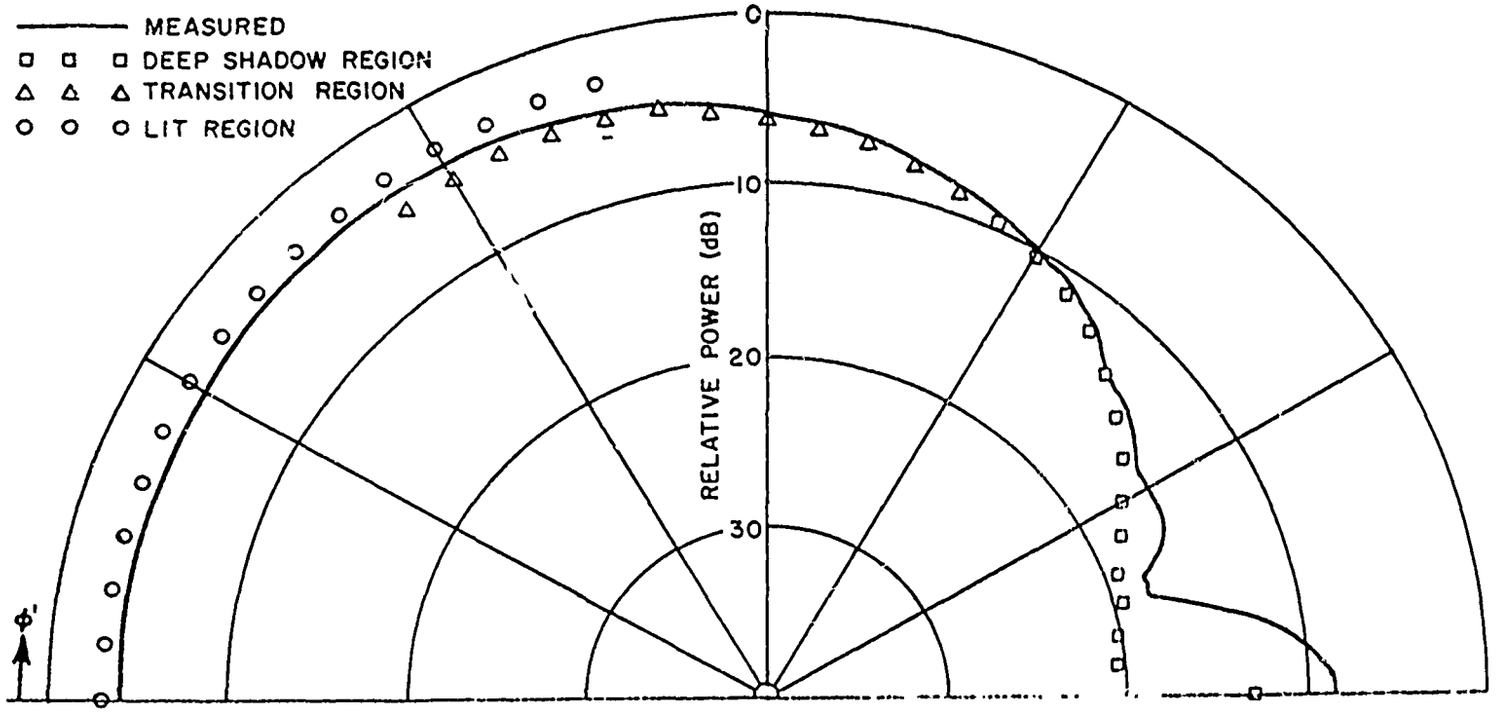

Fig. 18b. Off-principal plane pattern of monopole ($E_{\theta'}$) with ε=40°.

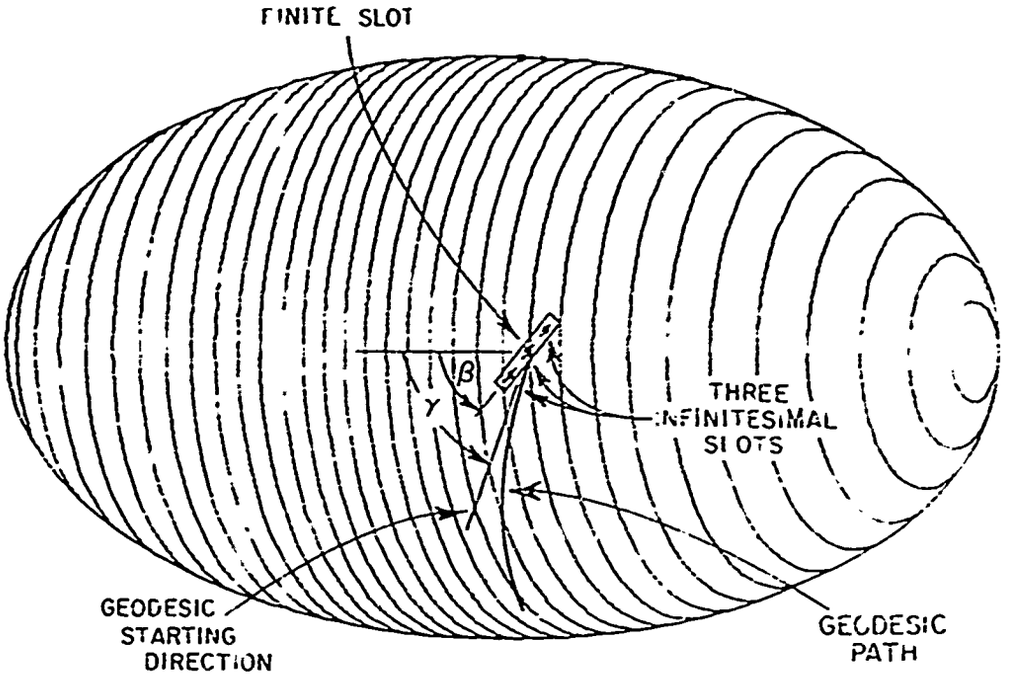

Fig. 19. Finite slot geometry.

the measured result as shown in Fig. 20 for a circumferential slot ($\beta = 90°$). Note that these results are again taken on a prolate spheroid. The calculated and measured off-principal plane patterns for $\xi = 20°$ and $40°$ are shown, respectively, in Figs. 21 and 22. In each case, good agreement is obtained between the measured and calculated results.

As stated earlier, the elevation plane pattern is a special case that must be considered using our new geodesic solution. To examine this case, an axial slot was mounted on our prolate spheroid and the elevation plane pattern measured at NADC. The results of this study are presented and compared with the two-dimensional elevation plane pattern in Fig. 23a and with the three-dimensional elevation plane pattern in Fig. 23b. It is immediately obvious that the back-lobe region is not calculated with sufficient accuracy using the two-dimensional result. However, the three-dimensional solution is in good agreement with the measured pattern.

Again the slot cases treated are rather idealized as compared to the more general problem originally outlined. However, off-principal plane radiation patterns from antennas mounted on three-dimensional surfaces which are large in terms of the wavelength have not been analytically computed with much success to date. Thus, one must begin by treating specific cases which are easily modelled and

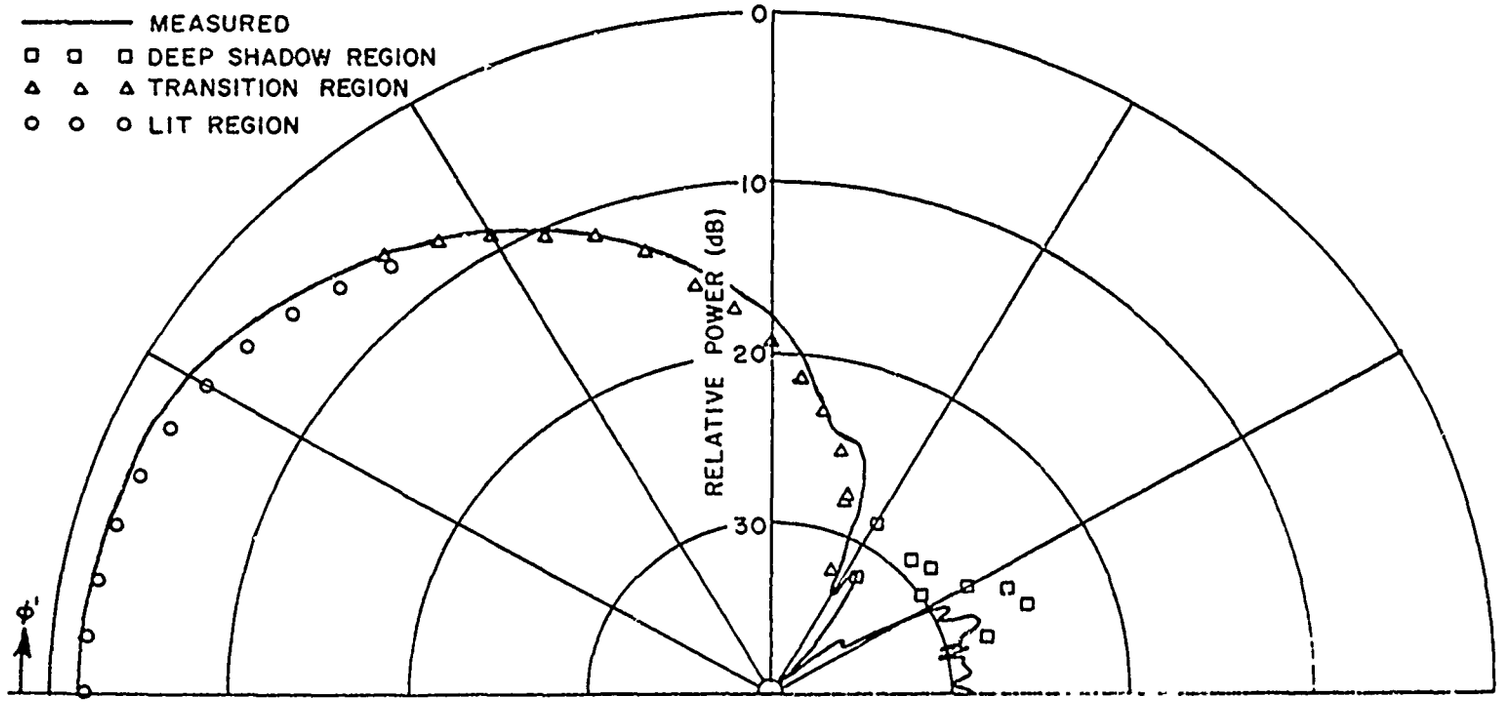

Fig. 20. Principal plane pattern of circumferential slot ($E_{\phi'}$) with ξ=0°.

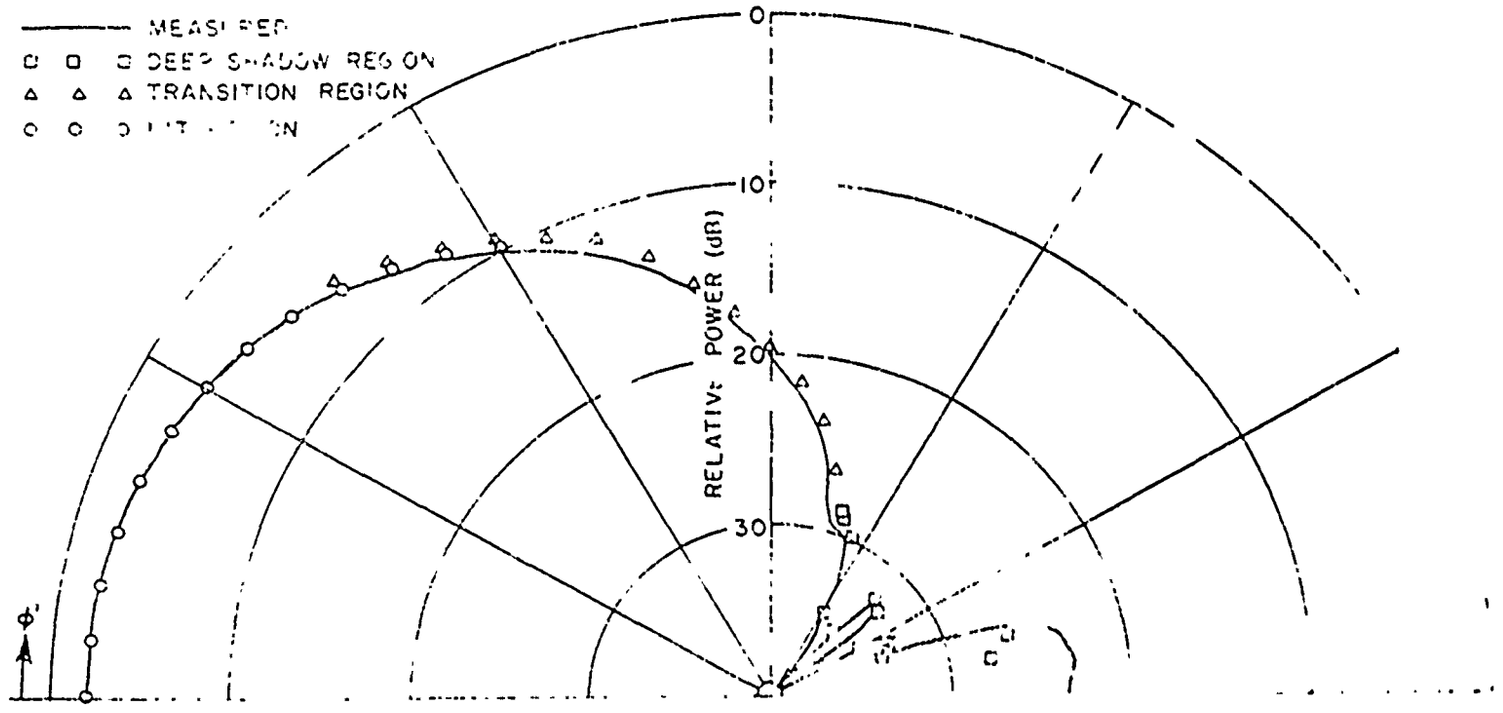

Fig. 21. Off-principal plane pattern of circumferential slot (E_{θ}) with γ=20°.

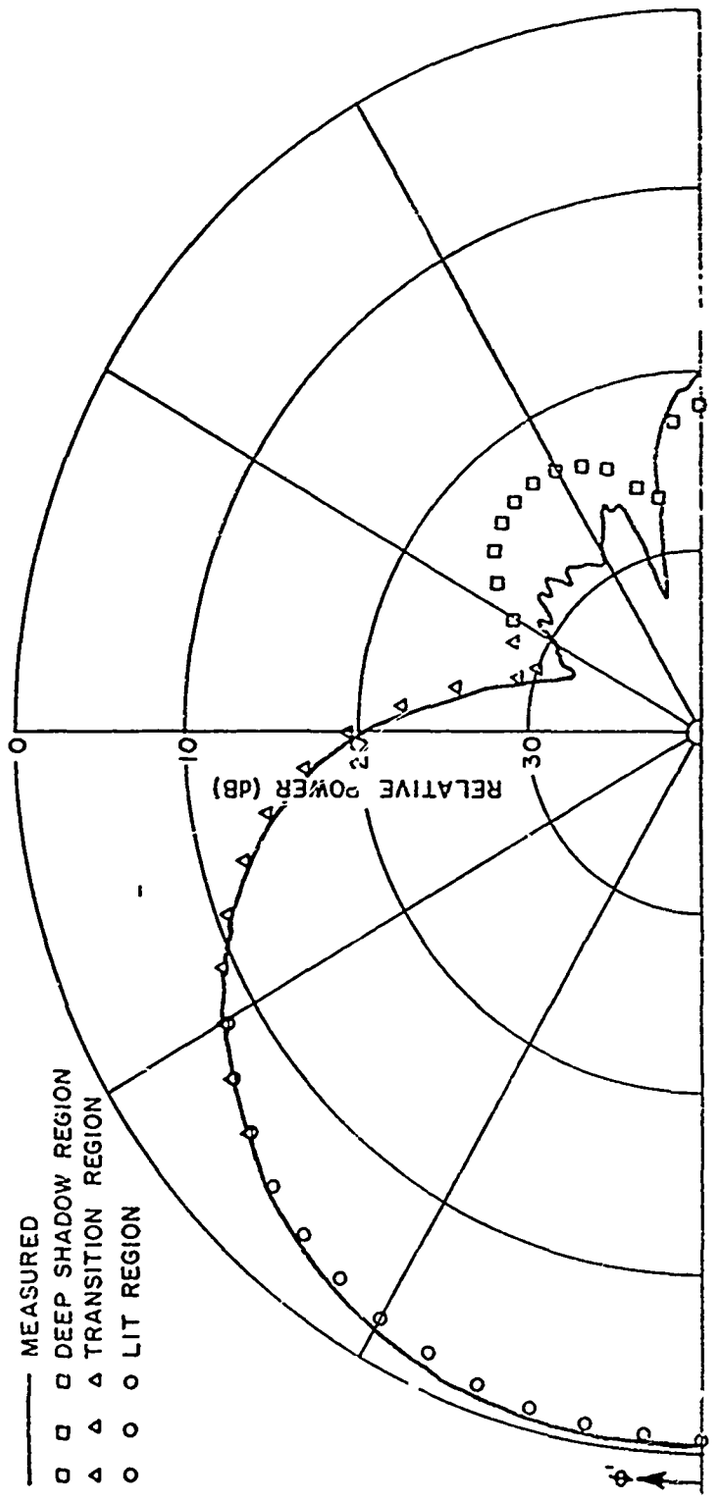

Fig. 22. Off-principal plane patterns of circumferential slot ($E_{\theta'}$) with ξ=40°.

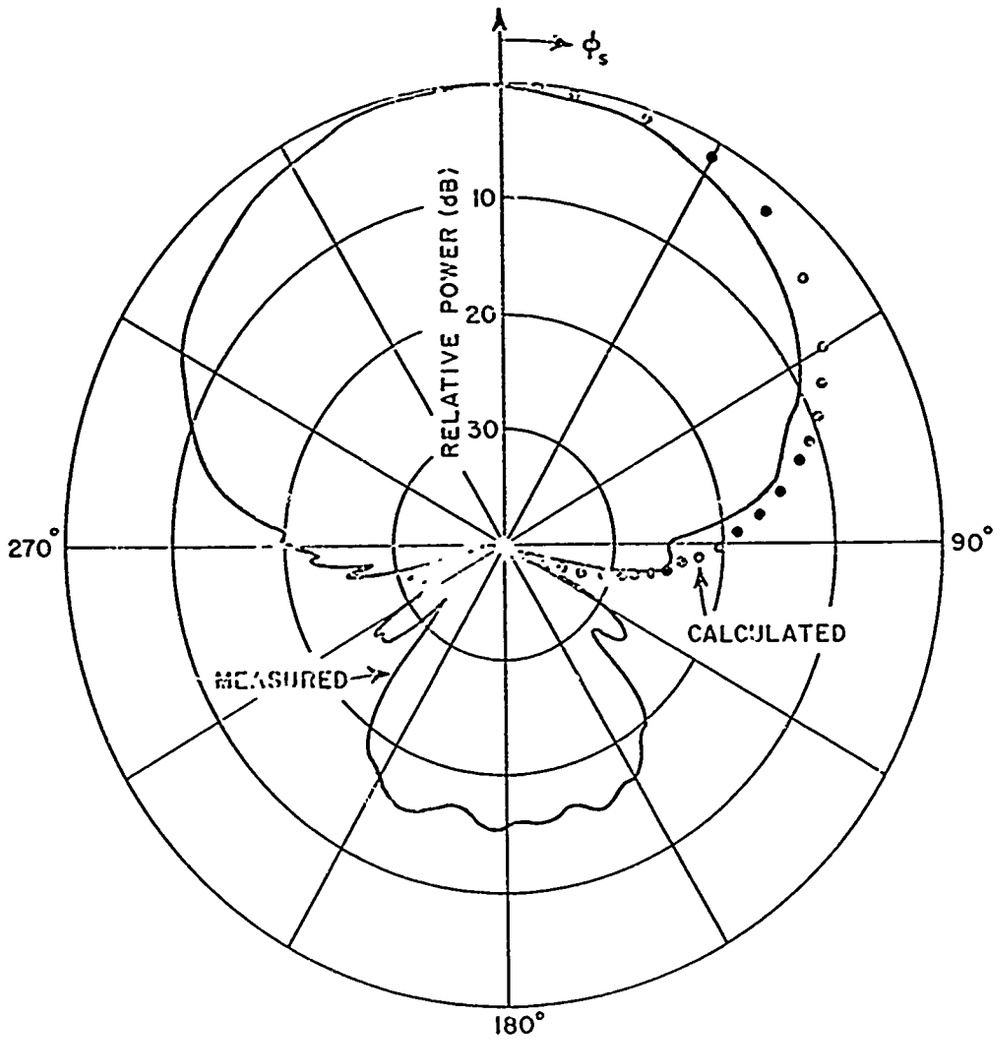

Fig. 23a. Elevation plane pattern of an axial slot mounted on a 4λ x 2λ prolate spheroid with the two-dimensional theoretical solution presented.

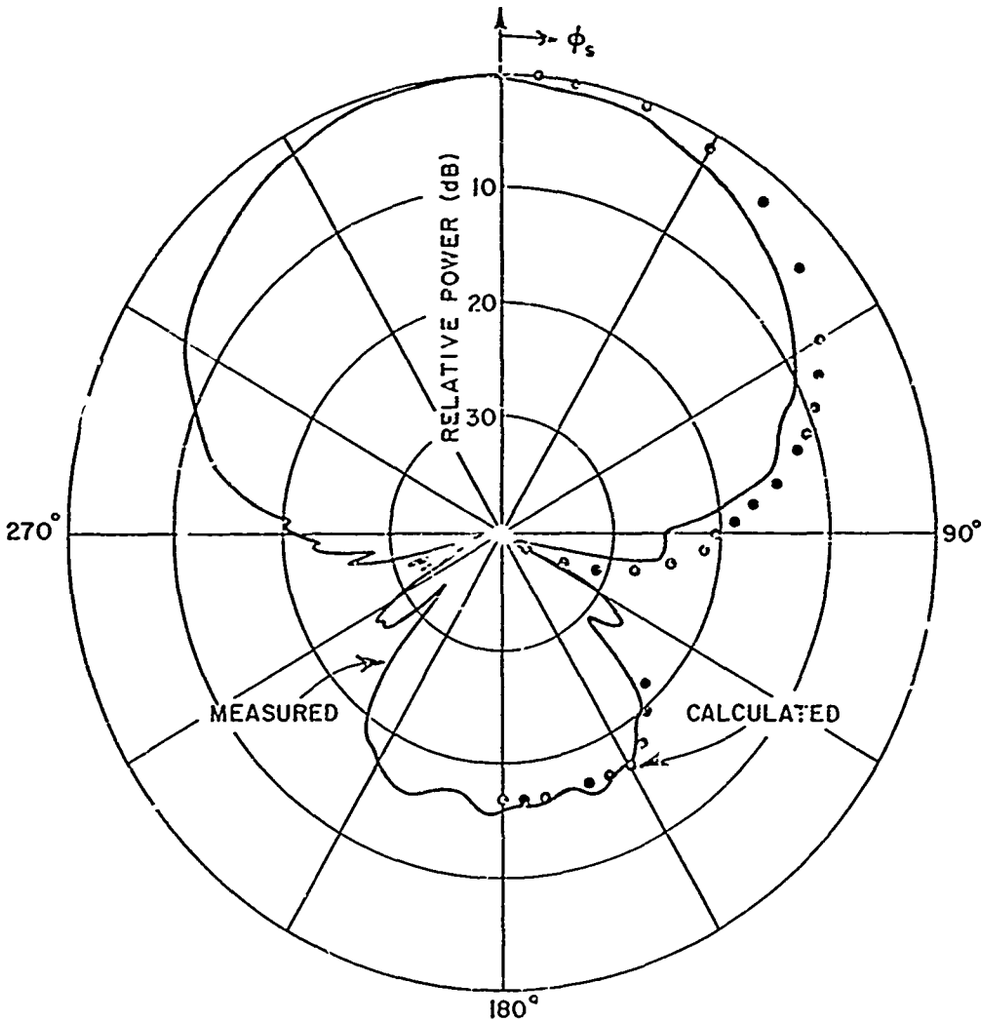

Fig. 23b. Elevation plane pattern of an axial slot mounted on a $4\lambda \times 2\lambda$ prolate spheroid with the three-dimensional theoretical solution presented.

computed. In this way one is able to ascertain the validity of his solution. The above results, then, indicate that the high frequency solutions of Kouyoumjian[28] can be applied at least to this idealized problem. One must, now, extend these solutions to determine for what type fuselage models they tend to break-down, if in fact they do.

IV. INTERACTIVE ON-AIRCRAFT ANTENNA PATTERN CALCULATIONS

The following discussion describes an interactive computer program written to illustrate the utility of computer aided design of on-aircraft antennas. Using this program there is immediate interaction between the engineer and computer in determining the optimum locations for antennas based on their roll plane pattern performance. A PDP-7 light-pen/CRT display unit is used for quick manipulation of the various parameters which affect the resulting pattern. A modified Data-craft 6024 is used for the pattern computations based on the model parameters defined by the light-pen/CRT design.

Upon initiating the program a master table of available options is displayed on the CRT as shown in Fig. 24. Control is passed to the desired subroutine by touching the light-pen on the desired parameter word and then touching the "FIX" in the lower right corner. Control is returned to the master table after completion of each sub-program and the unit is ready for a new command. By calling the subroutine "Antenna Type" through light-pen control the present antenna type mounted on the fuselage of the aircraft is indicated plus three options as shown in Fig. 25. The antenna type can be easily changed to any one of the three infinitesimal antennas using the light-pen. The change is immediately indicated.

The frequency of the case under investigation is indicated, as shown in Fig. 26, by calling the subroutine entitled "FREQUENCY". The arrow points to the present frequency on a linear frequency scale. The value of the frequency may be changed by relocating the vertical cross-wire line using the light-pen and then hitting the "FIX". The master table is returned and the frequency set by hitting the words "USE PRESENT VALUE".

The antenna location is identified by hitting "ANTENNA LOCATION" in the master table. The angular location of the antenna is illustrated first as shown in Fig. 27. It can be simply relocated using the cross-wires and light-pen. Secondly, the linear position (station) of the antenna is indicated as shown in Fig. 28 in a top view of the aircraft. The linear position may also be changed using the light-pen.

Using the subroutine entitled "WING GEOMETRY" one can easily modify the wing shape. An n-sided flat plate model is used to

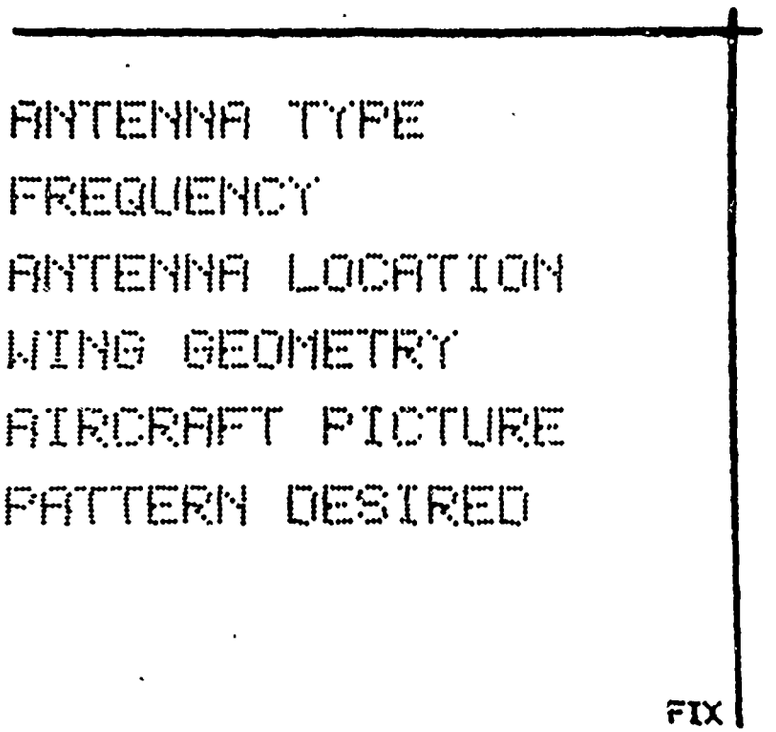

Fig. 24. Master table of available options.

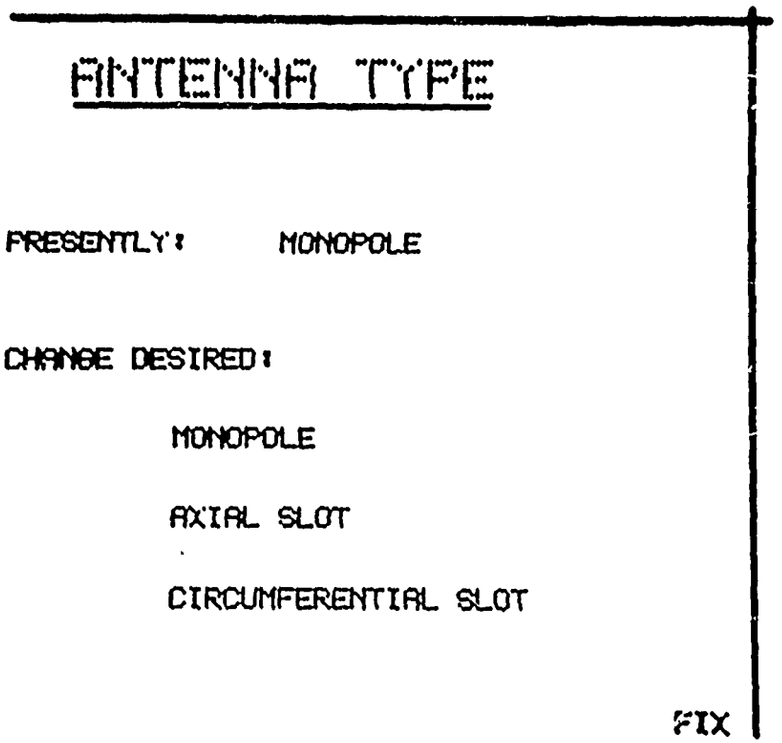

Fig. 25. Antenna type option.

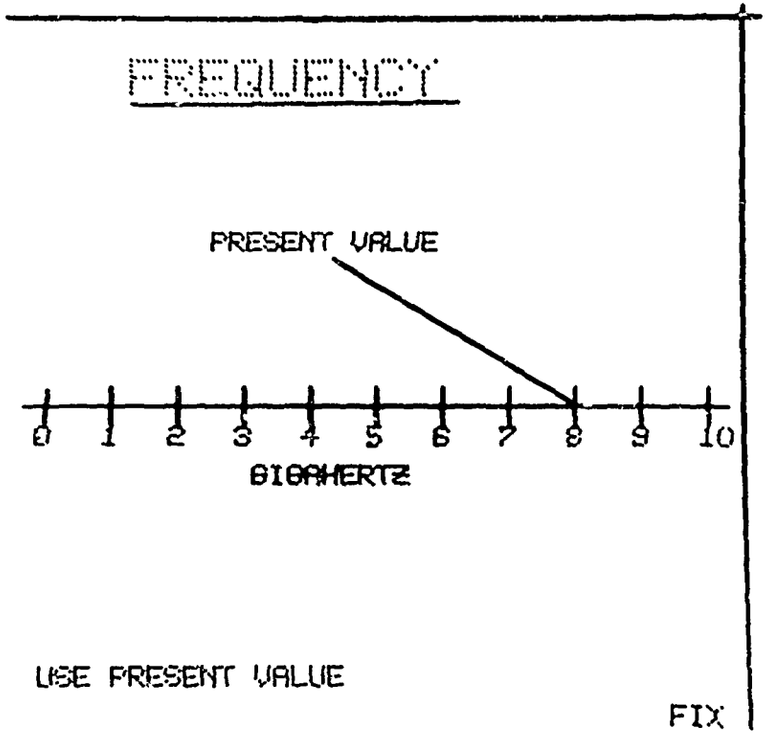

Fig. 26. Frequency under investigation.

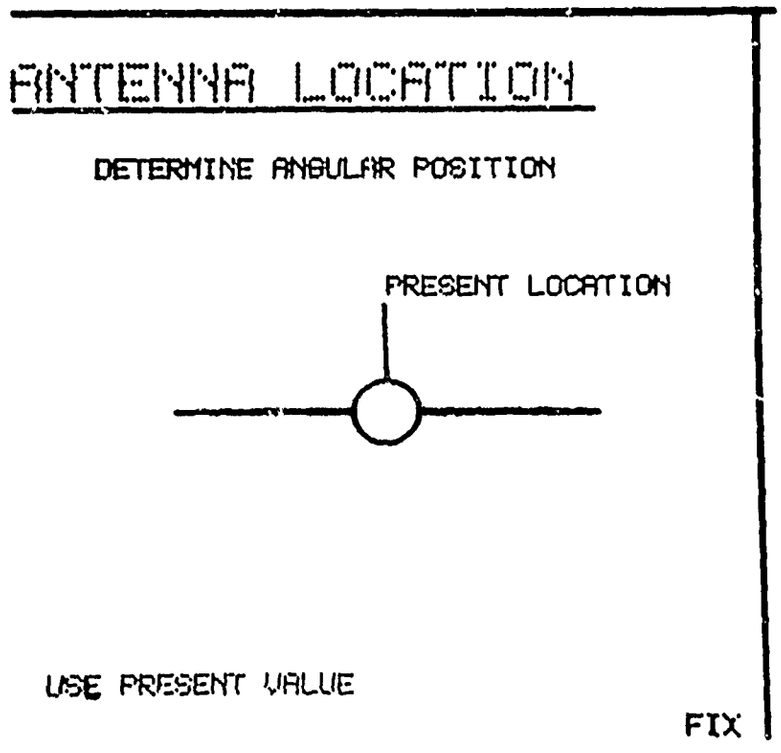

Fig. 27. Angular location of antenna.

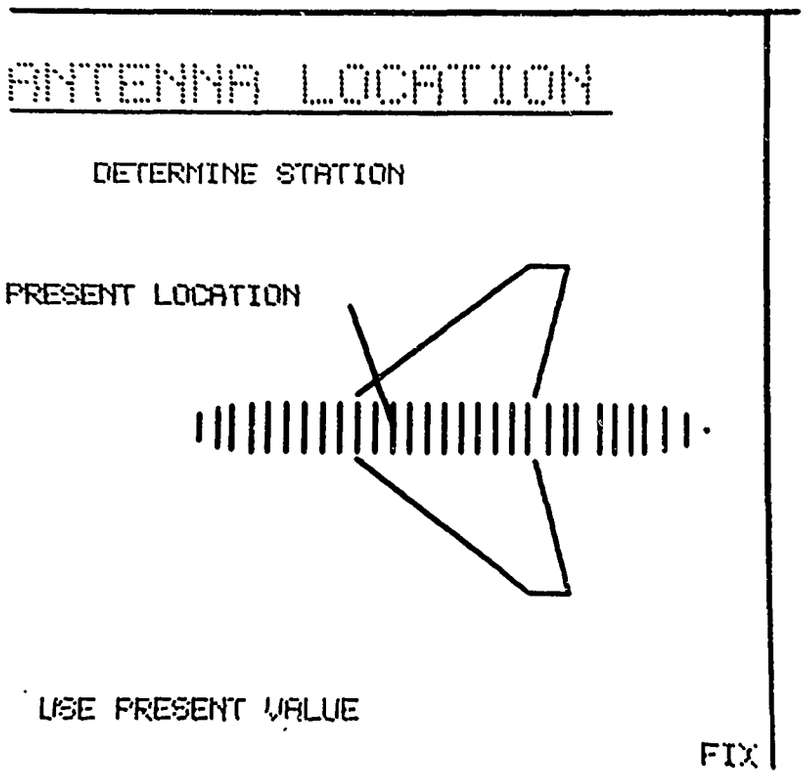

Fig. 28. Linear position of antenna with respect to wing location.

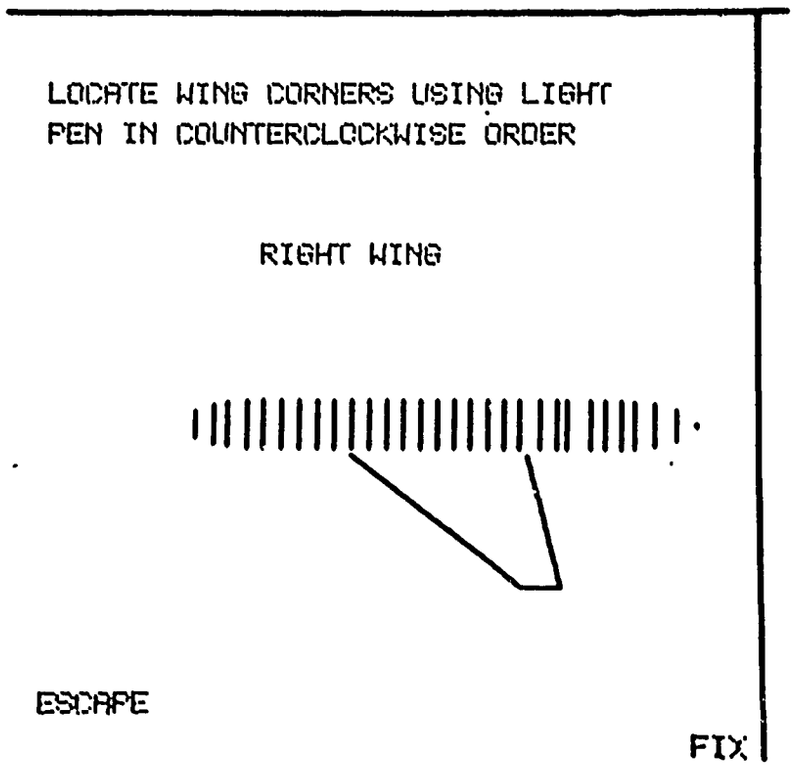

Fig. 29. Right wing geometry.

represent the wing. The corners of the wing model can be quickly redefined by locating the light-pen cross-wires at those points. The subroutine first illustrates the right wing, as shown in Fig. 29. Once the right wing is defined correctly, one has the option, under light-pen control, of defining the left wing differently or making it the image of the right wing as shown in Fig. 30. It is assumed for the purposes of this program that the wings are mounted in the horizontal plane which contains the fuselage axis. Our complete solution, however, is capable of handling wings mounted either above or below this central position.

The subroutine entitled "AIRCRAFT PICTURE" illustrates the aircraft configuration under investigation as illustrated in Fig. 31. The view is taken from above the aircraft toward the front.

By indicating the subroutine entitled "PATTERN DESIRED" the roll plane patterns for both theta and phi polarizations are computed for the previously defined aircraft-antenna configuration. The patterns are shown separately upon light-pen request and presented on a polar grid with 10 dB per division. The patterns are normalized to the maximum value for either polarization. The roll plane E-phi pattern, for the configuration shown in Fig. 31, is illustrated in Fig. 32. The E-theta pattern for the same case is shown in Fig. 33. Note that for a monopole the E-phi polarization is dominant, whereas, the E-theta gives the cross polarized pattern. Finally, the master table can be recalled, if desired, for further changes.

Using this approach the antenna engineers can sit at the console changing each of the parameters and obtaining various configurations which satisfy his needs. This information can, then, be used to bypass the need for extensive model measurements which are both expensive and time consuming.

V. CONCLUSIONS AND RECOMMENDATIONS FOR FURTHER RESEARCH

It has been shown in the previous sections that our solutions for the principal plane radiation patterns are quite good for the analytic models considered. It is obvious that the fuselage is the dominant scatterer; whereas, the wings and stabilizers are the main secondary contributors for the antenna locations studied. The present solutions are extremely versatile in terms of the analytic model representation, structure sizes and shapes, frequency, antenna locations, and antenna types. While we have been improving these solutions, the solution for the volumetric patterns for antennas on surfaces of revolution has been obtained. This solution additionally allows one to approximate the fuselage by a convex surface of revolution and determine the radiated field at any direction in space. This solution has been verified by measurements taken at The Ohio State University and at NADC.

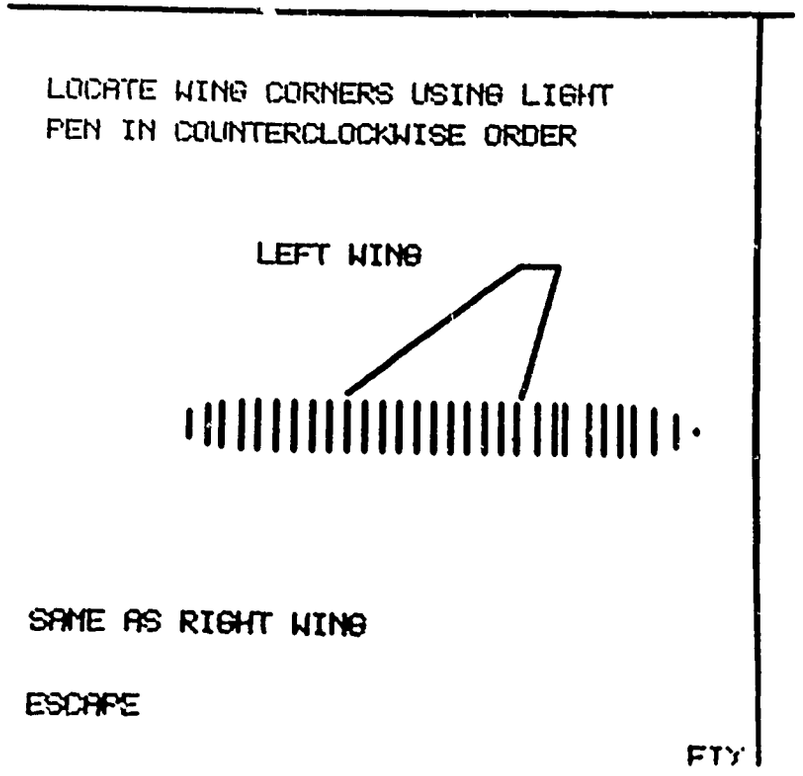

Fig. 30. Left wing geometry.

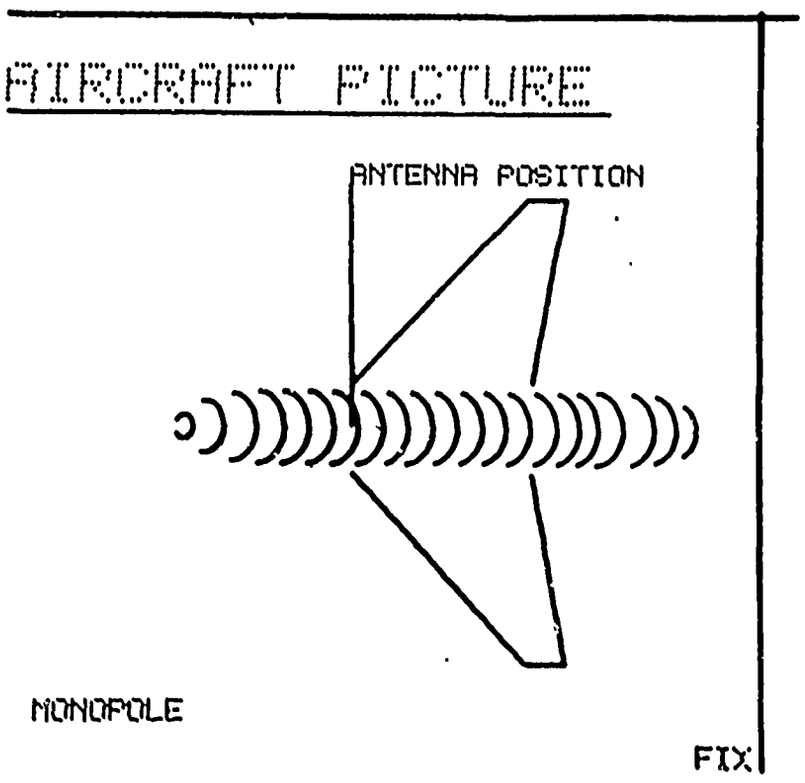

Fig. 31. View of complete configuration.

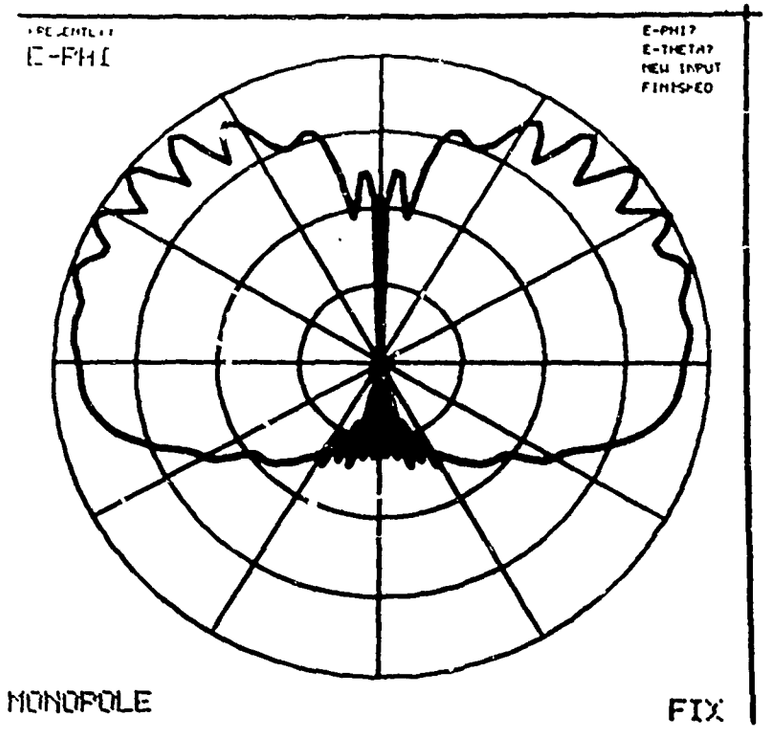

Fig. 32. E-phi roll plane pattern.

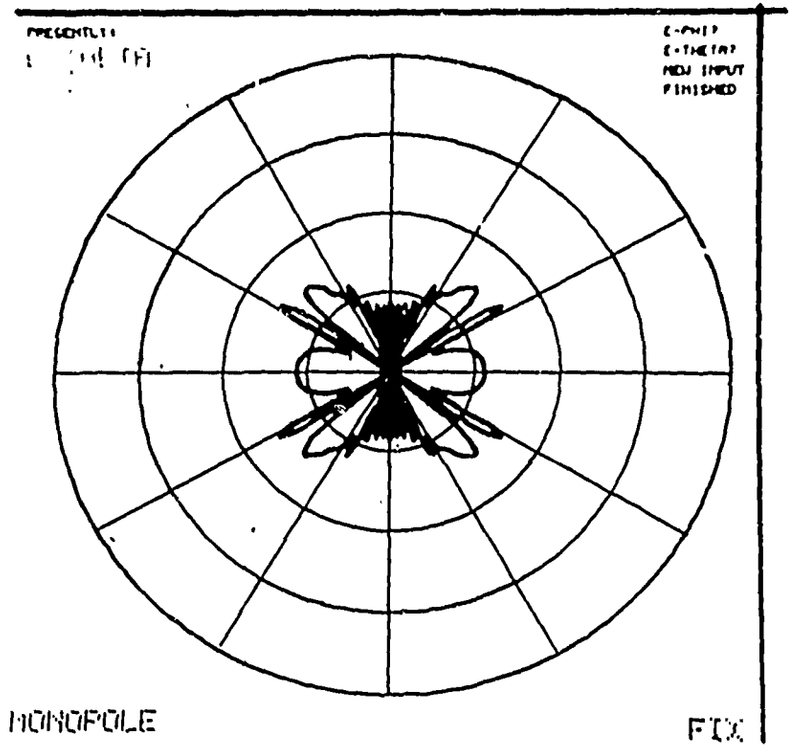

Fig. 33. E-theta roll plane pattern.

Since the volumetric pattern is very desirable, it is important that our initial study for antennas mounted on a surface of revolution be continued and improved upon. The most obvious next step is to include the main secondary scatterer, that being the wings. This can be accomplished using the near field flat plate scattering solution as was done in the roll plane. However, the addition of this solution for a surface of revolution is going to be a major effort. This solution will then give us a model which includes the dominant scattering terms and yet allows us to compute the pattern in arbitrary directions.

With the wings added to our three dimensional model one would next want to study just how adequate this analytic model is in practical situations for antennas mounted near the top or bottom of the aircraft. An experimental program to obtain data for verifying our analyses is now beginning at NADC. During this period, while experimental data are being obtained, a study of antennas mounted near the leading edge of the wing should begin. The effect of the scattering by the fuselage, especially in the azimuth plane, is important. To begin this study, the near field scattering by simple structures which approximate the fuselage should be determined.

REFERENCES

1. Carter, P.S., "Antenna Arrays Around Cylinders," Proc. IRE, Vol. 31, December, 1943, pp. 671-693.

2. Carter, P.S., "Antennas and Cylindrical Fuselage," Report No. 895-11, RCA Laboratories, Rocky Point, N.Y., December 24, 1943.

3. Sinclair, G., "The Patterns of Antennas Located Near Cylinders of Elliptical Cross Section," Proc. IRE, Vol. 39, No. 6, June 1951.

4. Richards, G.A., "A Boundary-Value Technique for Computing the Patterns of an Antenna Near a Conducting Body of Arbitrary Shape," Report 2235-2, 11 September 1967, The Ohio State University ElectroScience Laboratory, Department of Electrical Engineering; prepared under Contract No. N10019-67-C-0063 for Naval Air Systems Command.

5. Richmond, J.R., "Computer Analysis of Three-Dimensional Wire Antennas," Report 2708-4, 22 December 1969, The Ohio State University ElectroScience Laboratory, Department of Electrical Engineering; prepared under Contract DAAD 05-69-C-0031 for Ballistic Research Laboratory.

6. Lin, Y.T. and Ksienski, A.K., "Computation of Low Frequency Scattering from Airplanes," Report 2768-9, July 1972, The Ohio State University ElectroScience Laboratory, Department of Electrical Engineering; prepared under Grant AFOSR 69-1710 for Air Force Office of Scientific Research.

7. Ryan, C.E., Jr. and Rudduck, R.C., "Calculation of the Radiation Pattern of a General Parallel-Plate Waveguide Aperture for the TEM and TE_{01} Waveguide Modes," Report 1693-4, 10 September 1964, The Ohio State University ElectroScience Laboratory, Department of Electrical Engineering; prepared under Contract N62269-2184 for U.S. Naval Air Development Center, Johnsville, Pennsylvania.

8. Ryan, C.E., Jr. and Rudduck, R.C., "A Wedge Diffraction Analysis of the Radiation Patterns of Parallel-Plate Waveguides," IEEE Trans. on Antennas and Propagation Comm., Vol. Ap-16, No. 4, July 1968.

9. Wu, D.C.F., Rudduck, R.C. and Pelton, E.L., "Application of a Surface Integration Technique to Parallel-Plate Waveguide Radiation Pattern Analysis," IEEE Trans. Antennas and Propagation, Vol. AP-17, May 1969, pp. 280-285.

10. Burnside, W.D. and Pelton, E.L., "Wedge Diffraction Theory Analysis of Parallel-Plate Waveguide Arrays," Report 2382-14, 25 September 1969, The Ohio State University ElectroScience Laboratory, Department of Electrical Engineering; prepared under Contract F33615-67-C-1507 for the Air Force Avionics Laboratory, Wright-Patterson Air Force Base, Ohio.

11. Burnside, W.D., Pelton, E.L. and Peters, L., Jr., "Analysis of Finite Parallel-Plate Waveguide Arrays," to be published as a Communication in IEEE Trans. Antennas and Propagation.

12. Yu, J.S., Rudduck, R.C. and Peters, L., Jr., "Comprehensive Analysis for E-plane of Horn Antennas for Edge Diffraction Theory," IEEE Trans. Antennas and Propagation, Vol. AP-14, March 1966, pp. 138-149.

13. Yu, J.S. and Rudduck, R.C., "H-Plane Pattern of a Pyramidal Horn," IEEE Trans. on Antennas and Propagation Comm., Vol. AP-17, No. 5, September 1969.

14. Ratnasiri, P.A.J., Kouyoumjian, R.G., and Pathak, P.H., "The Wide Angle Side Lobes of Reflector Antennas," Report 2183-1, 23 March 1970, The Ohio State University ElectroScience Laboratory, Department of Electrical Engineering; prepared under Contract AF 19(628)-5929 for Air Force Cambridge Research Laboratories.

15. Mentzer, C.A., Pathak, P.H., and Peters, L., Jr., "Pattern Analysis of an Offset Fed Parabolic Reflector Antenna," Report 3220-2, June 1972, The Ohio State University ElectroScience Laboratory, Department of Electrical Engineering; prepared under Contract N00178-71-C-0264 for U.S. Naval Weapons Laboratory.

16. Ryan, C.E., Jr. and Rudduck, R.C., "Radiation Patterns of Rectangular Waveguides," IEEE Trans. Antennas and Propagation Comm., Vol. AP-16, July 1968, pp. 488-489.

17. Balanis, C.A. and Peters, L., Jr., "Analysis of Aperture Radiation from an Axially Slotted Circular Conducting Cylinder Using Geometrical Theory of Diffraction," IEEE T-AP-17, January 1969, pp. 93-97.

18. Balanis, C.A. and Peters, L., Jr., "Aperture Radiation from an Axially Slotted Elliptical Conducting Cylinder using Geometrical Theory of Diffraction," IEEE T-AP-17, July 1969, pp. 507-513.

19. Balanis, C.A. and Peters, L., Jr., "Radiation from TE_{10} Mode Slots on Circular and Elliptical Cylinders," IEEE T-AP-18, No. 3, May 1970, pp. 400-403.

20. Ryan, C.E., Jr., "Analysis of Radiation Patterns of Antennas on Finite Circular Cylinders and Conically-Capped Cylinders," Report 2805-2, 25 September 1970, The Ohio State University ElectroScience Laboratory, Department of Electrical Engineering; prepared under Contract DAA21-69-C-0535 for Picatinny Arsenal.

21. "Low-Profile Scanned-Beam IFF Antenna System Development Study," Final Report 2836-4, 11 August 1970, The Ohio State University ElectroScience Laboratory, Department of Electrical Engineering; prepared under Contract N62269-69-C-0533 for Naval Air Development Center.

22. Marhefka, R.J., "Roll Plane Analysis of On-Aircraft Antennas," Report 3188-1, December 1971, The Ohio State University ElectroScience Laboratory, Department of Electrical Engineering; prepared under Contract N62269-71-C-0296 for Naval Air Development Center.

23. Burnside, W.D., "Analysis of On-Aircraft Antenna Patterns," Report 3390-1, August 1972, The Ohio State University ElectroScience Laboratory, Department of Electrical Engineering; prepared under Contract N62269-72-C-0354 for Naval Air Development Center.

24. "On-Aircraft Antennas," Final Report 3188-3, January 1972, The Ohio State University ElectroScience Laboratory, Department of Electrical Engineering; prepared under Contract N62269-71-C-0296 for Naval Air Development Center.

25. Yu, C.L. and Burnside, W.D., "Elevation Plane Analysis of On-Aircraft Antennas," Report 3188-2, January 1972, The Ohio State University ElectroScience Laboratory, Department of Electrical Engineering; prepared under Contract N62269-71-C-0296 for Naval Air Development Center.

26. Kouyoumjian, R.G., "Asymptotic High-Frequency Methods," Proceedings of the IEEE, Vol. 53, No. 8, August 1965, pp. 864-876.

27. Struik, D.G., Differential Geometry, Addison-Wesley Press, Inc., Cambridge, Mass., 1950, pp. 127-134.

28. Pathak, P.H. and Kouyoumjian, R.G., "The Radiation from Apertures in Curved Surfaces," Report 3001-2, December 1972, The Ohio State University ElectroScience Laboratory, Department of Electrical Engineering; prepared under Grant NGR 36-008-144 for National Aeronautics and Space Administration.

29. Walter, C.H., Traveling Wave Antennas, Dover Publications, Inc., New York, 1970, pp. 15-16.